Porphyromonas gingivalis induces penetration of lipopolysaccharide and peptidoglycan through the gingival epithelium via degradation of coxsackievirus and adenovirus receptor

Hiroki Takeuchi (takeuchih@dent.osaka-u.ac.jp)
Osaka University
Shunsuke Yamaga
Osaka University
Naoko Sasaki
Osaka University
Masae Kuboniwa
Osaka University
Michiya Matsusaki
Osaka University
Atsuo Amano
Osaka University

Research Article

Keywords: Porphyromonas gingivalis, periodontal disease

Posted Date: February 23rd, 2021

DOI: https://doi.org/10.21203/rs.3.rs-181107/v1

Porphyromonas gingivalis induces penetration of lipopolysaccharide and peptidoglycan through the gingival epithelium via degradation of coxsackievirus and adenovirus receptor

Hiroki Takeuchi[1,4*], Shunsuke Yamaga[1,4], Naoko Sasaki[2], Masae Kuboniwa[1], Michiya Matsusaki[2,3], Atsuo Amano[1*]

1 Department of Preventive Dentistry, Graduate School of Dentistry, Osaka University, Suita-Osaka 565-0871, Japan

2 Joint Research Laboratory (TOPPAN) for Advanced Cell Regulatory Chemistry, Graduate School of Engineering, Osaka University, Suita-Osaka 565-0871, Japan

3 Department of Applied Chemistry, Graduate School of Engineering, Osaka University, Suita-Osaka 565-0871, Japan

4 These authors have contributed equally to this work

Short title: *CXADR prevents LPS and PGN penetration through gingival epithelium*

*Address correspondence to:

Hiroki Takeuchi, DDS, PhD, Assistant Professor: e-mail: takeuchih@dent.osaka-u.ac.jp

Atsuo Amano, DDS, PhD, Professor: e-mail: amanoa@dent.osaka-u.ac.jp

Department of Preventive Dentistry, Osaka University Graduate School of Dentistry,

1-8 Yamadaoka Suita-Osaka 565-0871, JAPAN

Tel: +81-6-6879-2921, Fax: +81-6-6879-2925

Abstract

Porphyromonas gingivalis is a major pathogen in severe and chronic manifestations of periodontal disease, which is one of the most common infections of humans. A central feature of *P. gingivalis* pathogenicity is dysregulation of innate immunity at the gingival epithelial interface. We previously showed that junctional adhesion molecule 1 (JAM1) was specifically degraded by *P. gingivalis,* leading to epithelial barrier breakdown in gingival tissues. Whereas, the involvement of the other JAM family protein(s) in the epithelial barrier dysregulation by *P. gingivalis* remains unknown. Here we show that Arg-specific or Lys-specific cysteine proteases named gingipains produced by *P. gingivalis* specifically degrade coxsackievirus and adenovirus receptor (CXADR), a tight junction associated protein, at R145 and K235 in gingival epithelial cells. A *P. gingivalis* strain lacking gingipains was impaired in degradation of CXADR. Knockdown of CXADR in a three-dimensional multilayered tissue model increased permeability to 40 kDa dextran, lipopolysaccharide, and proteoglycan. Inversely, overexpression of CXADR in a gingival epithelial tissue model prevented penetration by these agents following *P. gingivalis* infection. Our findings strongly suggest that *P. gingivalis* gingipains disrupt barrier function of stratified squamous epithelium via degradation of CXADR as well as JAM1, efficiently allowing bacterial virulence factors to penetrate into subepithelial tissues.

Main

Introduction

Periodontal diseases are chronic infectious diseases caused by complex actions of periodontal bacteria in oral biofilm, and one of the most common infectious diseases of humans [1]. In periodontal tissues, the subgingival epithelium responds to microbial infection and harmonizing innate immunity [2]. Lipopolysaccharide (LPS: endotoxins of gram-negative bacteria) and peptidoglycan (PGN: mesh-like patterns outside the plasma membrane of most bacteria) are prototypal classes of pathogen-associated molecular patterns (PAMPs) that are recognized by the innate immunity [3].

The epithelium lining gingival sulcus is stratified squamous. Gingival epithelial cells express molecular complexes regulating cell-to-cell adhesion [4]. Human gingival epithelial cells express junctional adhesion molecules (JAMs), members of an immunoglobulin superfamily, that seal the paracellular pathway and prevent solutes passing through the paracellular space [4,5]. Homodimerization of JAMs is important for regulating epithelial barrier function [6]. However, barrier function of the sole JAM family proteins in human epithelium remains largely unknown.

Porphyromonas gingivalis, a keystone periodontal pathogen, can impair host immune defense and promote inflammation [7]. *P. gingivalis* secrets Arg-specific and Lys-specific cysteine proteases, termed Arg-gingipains (RgpA and RgpB) and Lys-gingipain (Kgp), respectively, which possess abundant proteolytic activities [8,9]. Hence, host proteins targeted and degraded by gingipains could be considered crucial factors influencing pathogenesis of periodontitis. We previously identified JAM1 as a gingival epithelial barrier protein, which is specifically degraded by *P. gingivalis* gingipains, leading to epithelial barrier breakdown by allowing increased epithelial permeability to

PAMPs [10]. Whereas, the possibility that other JAM family proteins are targeted by *P. gingivalis* has not been verified. In this study, we screened the JAM family proteins involved in gingival epithelial barrier dysfunction by *P. gingivalis* using a three-dimensional multilayered tissue model (3D-tissue model). We consequently identified CXADR as an additional JAM family protein targeted specifically by the pathogen. Gingipains degrades CXADR at R145 and K235, thereby inducing gingival epithelial permeability and allowing subsequent transmission of LPS and PGN. This work provides insights into process by which gingival epithelial barrier is subverted during periodontal pathogenesis.

Results

P. gingivalis gingipains degrade CXADR in gingival epithelial cells

To elucidate the JAM1-independent mechanism of gingival epithelial barrier function, we screened eight JAM family proteins [6] for their expression in immortalized human gingival epithelial (IHGE) cells. For this purpose, we used reverse transcriptional polymerase chain reaction (RT-PCR), and found that JAM2, CLMP, and CXADR were expressed in IHGE cells in addition to JAM1 (Fig. 1a). While, the negligible expression of JAM3, JAM4, CD2, and ESAM was observed in IHGE cells. Next, we investigated whether gingipains degrade these JAM family proteins cell at the endogenous protein level. We infected IHGE cells with *P. gingivalis* ATCC33277 wild type (WT) or its isogenic mutant KDP136 (Δ*kgp* Δ*rgpA* Δ*rgpB*) for 1 h at a multiplicity of infection (MOI) of 100. We detected the decreased levels of JAM1, CXADR, and CLMP in IHGE cells were decreased by *P. gingivalis* WT, while the Δ*kgp* Δ*rgpA* Δ*rgpB* mutant had a negligible effect (Fig. 1b). By contrast, *P. gingivalis* did not degrade JAM2 at 1 h after infection.

These results suggest that gingipains specifically degrade JAM1, CXADR, and CLMP.

To assess the contribution of CXADR or CLMP expression to the permeability of gingival epithelial cells, we generated IHGE cell lines stably expressing small hairpin RNA (shRNA) against JAM1 (shJAM1 #110 and shJAM1 #508), CXADR (shCXADR #38 and shCXADR #317), and CLMP (shCLMP #661 and shCLMP #771), respectively. We then performed permeability assays using a small-molecule fluorescent probe (Fig. 2a). Knockdown of JAM1, CXADR, and CLMP in each cell line was confirmed by immunoblot (Fig. 2b). As shown in Figure 2c, IHGE monolayers expressing shRNA against CXADR as well as JAM1 were significantly more permeable to 40 kDa FITC-dextran, FITC-labeled *P. gingivalis* LPS, and FITC-labelled *P. gingivalis* PGN than control cells expressing shRNA against firefly luciferase (shLuc). By contrast, knockdown of CLMP had a negligible effect on the permeability to these tracers.

We examined the effects of secreted gingipains on CXADR in the same way that we previously studied the impact of gingipains on JAM1 [10]. The bacterial culture supernatant was collected and administered to IHGE cells for 1 h. We detected the decreased levels of CXADR in IHGE cells by the culture supernatant of *P. gingivalis* WT. By contrast, the Δ*kgp* Δ*rgpA* Δ*rgpB* mutant showed a negligible effect (Fig. S1). These results indicate that CXADR are degraded by secreted gingipains.

We next examined the association of *P. gingivalis* with CXADR in IHGE cells using a laser confocal microscope. At 1 h after infection of *P. gingivalis* WT the signal intensity of CXADR was reduced in the surface area of IHGE cells (Fig. 3a). By contrast, the Δ*kgp* Δ*rgpA* Δ*rgpB* mutant failed to reduce the CXADR signal, consistent with the results in Figure 1b and 1c. In order to examine the effects of gingipains on CXADR degradation in deeper epithelium, we created a 3D-tissue model of IHGE cells

by the cell-accumulation technique (Fig. 3b) [11]. We infected the 3D-tissue models with *P. gingivalis* WT or Δ*kgp* Δ*rgpA* Δ*rgpB,* and analyzed the CXADR degradation in deeper epithelium using confocal microscopy. At 2 h after infection, *P. gingivalis* WT is capable of reducing the CXADR signal even in the tissues 3–4 layers below the surface (Fig 3b). By contrast, the Δ*kgp* Δ*rgpA* Δ*rgpB* mutant failed to reduce the CXADR signal. These results suggest that gingipains deeply invade human gingival epithelial tissues and degrade CXADR.

CXADR is localized in the plasma membrane following cleavage of N-terminal signal peptide

We hypothesized that *P. gingivalis* gingipains degrades CXADR localizes on the plasma membrane, but not efficiently in intracellular space. CXADR has a predicted signal peptide followed by immunoglobulin (IG) domains and a transmembrane domain [12,13]. In order to test this hypothesis, we visualized the intracellular localization of CXADR before and after cleavage of its signal peptide. We created a plasmid encoding Myc–tagged human influenza hemagglutinin (HA)–inserted CXADR (Fig. 4a) and examined the localization of the chimeric protein in IHGE cells to determine by confocal microscopy. To monitor the CXADR localization, we stained IHGE cells expressing HA-tagged enhanced green fluorescent protein (EGFP) (Fig. S2a) or Myc–tagged HA-inserted CXADR (Fig. S2b) using anti-HA antibody, with or without permeabilization. We were able to label HA-EGFP protein with anti-HA antibody in the permeabilized IHGE cells, but not in the non-permeabilized cells, suggesting that the cytosolic proteins are not stained without permeabilization. By contrast, we were able to label HA-inserted CXADR protein with anti-HA antibody even without permeabilization,

suggesting that the ectopic protein of HA-inserted CXADR is properly transported to plasma membrane.

In order to trace the pathway(s) of CXADR, we next analyzed IHGE cells expressing Myc–tagged HA–inserted CXADR protein and each organelle marker: EGFP-SEC61β (marker for endoplasmic reticulum membrane protein); TOMM20 (marker for outer mitochondrial membrane protein; not included in endomembrane system) by confocal microscopy. We detected co-localization of the anti-Myc and anti-HA signals with SEC61β (Fig. 4b), but not TOMM20 (Fig. S3), suggesting that CXADR is transported via an endomembrane pathway. Additionally, phalloidin-stained actin in the peripheral area of IHGE cells co-localized with anti–HA-labeled CXADR, but not the Myc signal (Fig. 4c). These results suggest that the signal peptide of CXADR is cleaved at the endoplasmic reticulum and transported to the plasma membrane, and that gingipains are capable of targeting mature form of CXADR at cell surface.

P. gingivalis, but not _S. gordonii_ or _F. nucleatum_, degrades CXADR

In order to examine whether *P. gingivalis* degrades the immature and mature CXADR, we infected IHGE cells expressing Myc–tagged HA–inserted CXADR, and the kinetics of Myc- and HA-tagged CXADR were analyzed. Considering the substrate specifically of a gingipains property, we utilized the HA tag as a marker of mature CXADR because K or R residues are not included in HA amino acid sequence (YPYDVPDYA). In addition, we distinguished immature and mature CXADR in immunoblots by the N-terminal Myc tag. As shown in Figure 5a, *P. gingivalis* infection decreased the amount of mature CXADR labeled with anti-HA, but failed to decrease on the level of immature CXADR labeled with anti-Myc. These results suggest that mature form of CXADR are

targeted by *P. gingivalis*. In order to examine the effects of another *P. gingivalis* strain, we infected IHGE cells with *P. gingivalis* TDC60 isolated from a severe periodontal lesion [14]. At 1 and 2 h after infection, *P. gingivalis* TDC60 markedly reduced mature from of CXADR (Fig 5b), indicating that other *P. gingivalis* strain is capable of degrading CXADR.

Human oral bacteria including *Fusobacterium nucleatum* and *Streptococcus gordonii* can establish mixed-species communities leading to periodontopathic biofilm formation. [15]. In order to examine the effects of *S. gordonii* or *F. nucleatum* on CXADR, we infected IHGE cells expressing Myc–tagged HA–inserted CXADR with these species. As shown in Figure 5c and 5d, *S. gordonii* and *F. nucleatum* fail to reduce the level of HA–inserted CXADR at 2 h after infection, suggesting that CXADR cannot be degraded by *S. gordonii* and *F. nucleatum*.

CXADR R145 and K235 are responsible for degradation by *P. gingivalis*

In order to examine which residue(s) are responsible for degradation by *P. gingivalis* gingipains, we constructed plasmids encoding deleted and mutated CXADR and performed a structural analysis (Fig. 6a). We transfected these plasmids into IHGE cells and then infected cells with *P. gingivalis*. To detect the residue(s) targeted by gingipains, we replaced the R and K residues with H, a basic amino acid, in point mutation constructs. As shown in Figure 6b, degradation was observed in CXADR full length, CXADR Δ(1–234), but not JAM1 Δ(1-234) K235H, indicating that K235 is responsible for bacterial degradation. Additionally, the level of HA-tagged CXADR Δ(1–225) K235H and CXADR Δ(1–225) R226H K235H were not decreased by the infection, indicating that R226 is not responsible for bacterial degradation. Furthermore, the level of HA-tagged

CXADR Δ(1–144) K235H was reduced following infection with *P. gingivalis*, but CXADR Δ(1–144) R145H K235H was not. These results illustrate that R145 and K235 are the residues targeted for degradation by gingipains.

CXADR prevents penetration of LPS and PGN through gingival epithelium

It is previously reported that CXADR mediates homotypic cell adhesion in Chinese hamster ovary (CHO) cells [16]. However, the barrier function of CXADR in human squamous epithelium remains unknown. To assess the contribution of CXADR expression to the permeability of gingival deeper epithelium, we generated a 3D-tissue model stably expressing shLuc or shCXADR using the cell accumulation technique, and then performed permeability assays using a small-molecule fluorescent probe (Fig. 7a). Effective suppression of CXADR expression was confirmed by confocal microscopy (Fig. 7b). As shown in Figure 7c, IHGE monolayer expressing shRNA against CXADR was significantly more permeable to 40 kDa FITC-dextran than control cells expressing shLuc. This result suggests that CXADR is involved in the kinetics of flux of molecules with 40 kDa between gingival epithelial cell layers.

We previously showed that JAM1 prevented permeation to dissociated LPS and PGN monomer (N-acetylglucosamine-N-acetylmuramic acid) in the 3D-tissues of gingival epithelium [10]. This result prompted us to examine whether knockdown of CXADR allows permeation of LPS and PGN. Thirty minutes after administration, we detected the increased permeability to FITC-*P. gingivalis* LPS (Fig. 7d) and FITC-*P. gingivalis* PGN (Fig. 7e) by knockdown of CXADR. In order to confirm the generality of permeation of LPS and PGN following knockdown of CXADR, we also performed the permeability assay of *Escherichia coli* LPS and *Staphylococcus aureus* PGN through

gingival epithelial tissues. In tissues expressing shCXADR, we detected the increased permeability to FITC–*E. coli* LPS (Fig. 7d) and FITC–*S. aureus* PGN (Fig. 7e) at 30 min after administration, suggesting that CXADR affects the permeability of gingival epithelium to LPS and PGN.

Epithelial barrier function is regulated by CXADR independently of JAM1

As CXADR and JAM1 are of JAM family protein [6], these two proteins may interact with each other to mediate its localization in surface of gingival epithelial cells. To assess the interdependence of CXADR and JAM1, we determined the localization of CXADR and JAM1 in IHGE cells expressing shCXADR #317 or shJAM1 #508 by confocal microscopy. As shown in Figure S4a, the localization of JAM1 in IHGE monolayer expressing shJAM1 was negligible, but was not disturbed in IHGE cells expressing shCXADR. In the same trend, the expression level of CXADR in IHGE monolayer expressing shCXADR was negligible, but was not disturbed in IHGE cells expressing shJAM1 (Fig. S4b). These results suggest that CXADR and JAM1 are not interdependent on localization in gingival epithelial cells.

To assess the interdependence of CXADR and JAM1 on each localization in gingival epithelium, we generated the 3D-tissue models of IHGE cells expressing shCXADR and shJAM1 and the localiation of deeply seated CXADR and JAM1 was analyzed using confocal microscopy. The expression levels of IHGE cells expressing shCXADR and shJAM1 were confirmed by immunoblots (Fig. 8a). As shown in Figure 8b, shJAM1 caused JAM1, but not CXADR, to disappear even in the tissues 3–4 layers below the surface. In the same trend, shCXADR caused CXADR, but not JAM1, to disappear in the tissues below the surface. Finally, double knockdown of shCXADR and shJAM1

caused these two proteins to disappear in the tissues. These results suggest that the localization of CXADR and JAM1 are not interdependent even in gingival epithelium model. As shown in Figure 8c, depletion of either CXADR or JAM1 enhances permeability of gingival epithelium to 40 kDa dextran, and depletion of both CXADR and JAM1 showed an additional effect. These results show that CXADR mediates barrier function of gingival epithelium independently of JAM1.

CXADR degradation is involved in penetration of gingipains through gingival epithelial barrier

We previously showed that JAM1 degradation by gingipains is required for gingipains penetration in gingival epithelial cells [10]. In order to examine the CXADR-dependent mechanism of gingipains penetration, we employed a two-layered cell culture model, by which we can detect penetration of gingipains from the upper to the lower space (Fig. 9a). Six hours after administration of bacterial culture media, we confirmed the decreased level of HA-inserted CXADR, but not Myc-tagged CXADR, in the cells of the lower layer by *P. gingivalis* WT to a greater extent than by the Δ*kgp* Δ*rgpA* Δ*rgpB* mutant (Fig. 9b). Next, we examined whether overexpression of CXADR, the expression level of which compensates CXADR degradation by *P. gingivalis*, blocks the loss of CXADR in gingival epithelial cells. To test this idea, we employed two-layered culture of IHGE cells overexpressing CXADR, and the localization of CXADR in cells of the lower layer were monitored following *P. gingivalis* infection. When IHGE cells overexpressing CXADR were treated with bacterial culture media of *P. gingivalis* for 30 min, we detected the remaining CXADR proteins at almost the same level as in non-treated IHGE cells (Fig. S5), suggesting that degradation can be compensated by overexpression of CXADR

in this system. In line with this result, 6 h after administration, we detected the increased levels of HA-inserted CXADR in the lower layer when the cells in the upper layer overexpressed CXADR (Fig. 9b). These results indicate that degradation of CXADR by gingipains is important for penetration of the proteases through gingival epithelial cells.

Degradation of CXADR by *P. gingivalis* causes penetration of LPS and PGN

Next, we generated 3D-tissue model using IHGE cells overexpressing CXADR (Fig. 10a). We confirmed that marked amounts of CXADR were remained even in tissues infected with *P. gingivalis* (Fig. 10b). In order to examine the permeability, the tissues were then treated with 40 kDa FITC-dextran, FITC–*P. gingivalis* LPS, or FITC–*P. gingivalis*-PGN. Thirty minutes after administration, we detected the decreased permeability to 40 kDa FITC-dextran (Fig. 10c), FITC–*P. gingivalis* LPS (Fig. 10d), FITC–*P. gingivalis* PGN (Fig. 10e), FITC–*E. coli* LPS (Fig. 10f), and FITC–*S. aureus* PGN (Fig. 10g) in gingival epithelial tissues overexpressing CXADR. These results indicate that CXADR degradation by *P. gingivalis* is key for allowing the penetration of LPS and PGN in gingival epithelium.

Discussion

Our findings clearly suggest a molecular basis for the dysfunction of gingival epithelial barrier by *P. gingivalis*. Based on our results, we postulate the following model (Fig. 11). As CXADR as well as JAM1 localizes in a phalloidin-stained plasma membrane region in the 3D-tissue (Fig. 8b), CXADR and JAM1 function together as gingival epithelial barrier. By degrading not only JAM1 but also CXADR, *P. gingivalis* efficiently allows penetration of LPS, PGN, and gingipains derived from itself and other

284 bacteria through the gingival epithelium and into deeper periodontal tissues. In this
285 manner, *P. gingivalis* is probably able to destroy the epithelial barrier, which remotely
286 causes alveolar bone loss.

287 In this study, we employed a 3D-tissue model using the cell-accumulation technique
288 by a single cell coating with fibronectin/gelatin nanofilms [11]. We were able to
289 generate gingival epithelium even with knockdown of CXADR and JAM1 (Fig. 8b),
290 indicating that CXADR and JAM1 are not necessary for reconstruction of gingival
291 epithelium. Hence, the cell-accumulation technique is likely useful for defining
292 function of JAMs in the other types of epithelium.

293 We also generated HA-inserted CXADR for use as a probe in gingival epithelial cells.
294 Using an HA-tagged protein, we were able to detect the responsible amino acid residues
295 to bacterial degradation. *P. gingivalis* gingipains degrade CXADR at K235 (Fig. 6), and
296 JAM1 at R234 [10]. The hinge region between the C-terminal IG-like domain and the
297 transmembrane domain, possessing CXADR K235 and JAM1 R234, does not contain a
298 consensus sequence for N-glycosylation or secondary structure including helix, β-sheet,
299 and turn (Uniplot, JAM1: https://www.uniprot.org/uniprot/Q9Y624; CXADR:
300 https://www.uniprot.org/uniprot/P78310). Considering that the N-terminal IG-like
301 domain of CXADR and JAM1 is responsible for homodimerization [21,22], gingipains
302 effectively separate the N-terminal region away from the transmembrane domain.

303 We confirmed that single knockdown of CXADR or JAM1 increases permeability of
304 gingival epithelial tissues to 40 kDa dextran almost at the same level (Fig. 8c).
305 Additionally, double knockdown of CXADR and JAM1 in gingival epithelial tissues
306 showed further increase of permeability compared to single knockdown (Fig. 8c).
307 Upregulated CXADR or JAM1 messenger RNA expression is inhibited by the AP-1 or

the NF-κB inhibitor, respectively [23,24]. These multiple transcription pathways of CXADR and JAM1 may provide gingival epithelium a robust defense against external bacterial stress. Gingival epithelial function to control the barrier permeability is a perspective that should be further investigated in the etiology of periodontal disease.

Based on the results of this study, there remain at least two questions that we should consider in the future. One is whether other major pathogens could specifically degrade CXADR and JAM1. The increase in the amount of the "red complex" species (*P. gingivalis*, *Treponema denticola*, and *Tannerella forsythia*) in subgingival biofilms has been shown to be highly associated with the initiation and progression of periodontitis [17]. *T. denticola* expresses the serine protease, dentilisin and oligopeptidase B [18, 19]. *T. forsythia* expresses the cysteine protease, forsythia detachment factor [20]. The effects of these proteases on CXADR and JAM1 will be further examined.

The other one is the relationship between protein structure and the degradation. We showed that CXADR and JAM1, but not Claudin (CLDN) 1 and CLDN 4, were degraded by *P. gingivalis* in gingival epithelial cells [10]. JAM family proteins possess a single transmembrane domain, while CLDN family proteins are of a tetra spans transmembrane protein and possess two extracellular loops [5]. Accordingly, it is necessary to study other gingipains-degradative proteins which potentially regulates gingival epithelial barrier without an extracellular loop.

Methods (<1500 words)

Bacteria and cell culture

P. gingivalis ATCC 33277 (purchased from the American Type Culture Collection), TDC60 (kindly provided by Kazuyuki Ishihara, Tokyo Dental College), and KDP136 (Δ*kgp* Δ*rgpA* Δ*rgpB*, kindly provided by Koji Nakayama, Nagasaki University) [25] were maintained anaerobically on blood agar plates (BD) and grown in trypticase soy broth (BD), supplemented with hemin (5 μg mL^{-1}; WAKO), and menadione (1 μg mL^{-1}; Sigma-Aldrich). *S. gordonii* ATCC 35105 were grown aerobically at 37 °C in Todd-Hewitt broth. *F. nucleatum* subsp. *nucleatum* ATCC 25586 were grown anaerobically at 37°C on blood agar plates (BD). IHGE cells (kindly provided by Shinya Murakami, Osaka University) were maintained in Humedia KG-2 (Kurabo), as described previously [26]. For the preparation of the bacterial culture supernatant of *P. gingivalis*, the bacterial culture at a stationary growth phase was centrifuged at 3,300 *g* for 3 min, and the supernatant was collected and administered into the culture media of IHGE cells at a ratio of 1:50.

Reverse transcriptional PCR

Total RNA was extracted from IHGE cells using TRIzol (Thermo Fisher Scientific). Complementary DNA was synthesized using the iScript cDNA Synthesis Kit (Bio-Rad). Reverse transcriptional PCR was performed with the primers as follows: JAM1 forward, 5'-GTGCCTTCAGCAACTCTTCC-3'; reverse, 5'-ACCAGATGCCAAAAACCAAG-3'. JAM2 forward, 5'-TGCTCTGAGTGGAACTGTGG-3'; reverse, 5'-CACCTGCGATATCCAACAGA-3'. JAM3 forward, 5'-CAGACAAGTGACCCCAGGAT-3'; reverse, 5'-CAGCGATAAAGGGCTGAGTC-3'.

JAM4 forward, 5'-TCAAAGTGCAGTGAGCATCC-3'; reverse, 5'-CCCCAAGTAGGCAATGAAAA-3'. CD2 forward, 5'-CAGCCTGAGTGCAAAATTC-3'; reverse, 5'-CTCTGTGGGCTCTTGTCTCC-3'. CLMP forward 5'-CAGGAGCAGTGACAGGCATA-3'; reverse, 5'-TATTTGCTGTGGAGCGAGTG-3'. ESAM forward, 5'-GCCCTTTGTGATGTGGTTCT-3'; reverse, 5'-TTGCCTTGTTTGTCTTGCAC-3'. CXADR forward, 5'-ATGCCCACTTCATGGTTAGC-3'; reverse, 5'-GCGCTAGAGCAAGCAAAGTT-3'.

Cell accumulation technique

Three-dimensional culture of IHGE cells was performed as described previously [10]. IHGE cells collected by centrifugation after trypsinization were alternatively incubated for 1 min with 0.2 mg mL^{-1} fibronectin (Sigma-Aldrich) and 0.1% (w/v) gelatin (Nacalai Tesque) dissolved in phosphate-buffered saline (PBS). After each procedure, cells were washed with PBS (pH = 7.4) by centrifugation at 180 *g* for 2 min to remove unabsorbed polymers. After nine steps of immersion, fibronectin/gelatin nano-films were coated onto single-cell surfaces. A total of 2×10^6 cells coated with fibronectin/gelatin nano-films were seeded on coverslips coated with 0.2 mg mL^{-1} fibronectin dissolved in PBS in 24-well plates (Iwaki). After 36 h of incubation, tissues were subjected to experiments, fixed, and analyzed on a confocal microscope (TCS SP8; Leica Microsystems). The number of *P. gingivalis* cells in culture media were adjusted to an optical density at 600 nm of 0.12 to infect gingival epithelial tissues.

Antibodies and reagents

Mouse monoclonal anti–c-Myc (M4439), mouse monoclonal anti-HA (H3663), mouse monoclonal anti-JAM1 (SAB4200468), and mouse monoclonal β-ACTIN (A2228) antibodies were from Sigma-Aldrich; rabbit monoclonal anti-CXADR (10799-R271) was from Sino Bilogical; rabbit polyclonal anti-JAM2 (12972-1-AP) and rabbit polylonal anti-CLMP (16127-1-AP) was from Proteintech; rabbit monoclonal anti-HA antibody (3724) was from Cell Signaling Technology; rabbit monoclonal anti-TOMM20 (ab78547) was from Abcam. FITC–conjugated secondary (goat anti–mouse IgG, A-11001) antibody (MBL), and Alexa Fluor 488–conjugated secondary (goat anti–rabbit IgG, A11008), Alexa Fluor 568–conjugated secondary (goat anti–mouse IgG, A-11004), and Alexa Fluor 635–conjugated secondary (goat anti–rabbit IgG, A-31576) antibodies (Invitrogen) were used for fluorescence microscopy. Goat anti-mouse (7076) and anti-rabbit (7074) antibodies conjugated to horseradish peroxidase (Cell Signaling Technology) were used for immunoblotting. 4',6-diamidino-2-phenylindole (DAPI) (D1306, Invitrogen), Alexa Fluor 568– and Alexa Fluor 633–conjugated phalloidin (A12380 and A22284, respectively, Invitrogen) were used to stain IHGE cells.

Plasmids

The plasmid encoding Myc–tagged HA–inserted CXADR was constructed by cloning PCR products amplified from IHGE cells into pCMV-Myc (Clontech), using exogenously added *Eco*RI and *Kpn*I sites. To produce HA–inserted CXADR, DNA sequence of HA-tag was inserted into *CXADR* with fusion PCR. Plasmids encoding HA–tagged CXADR deletion mutants and point mutations were constructed by PCR. The plasmid encoding EGFP-SEC61β was constructed by cloning PCR products amplified from IHGE cells into pEGFP-C1 (Clontech). PCR amplification was performed with KOD Plus Neo

(Kurabo). PCR products were ligated into plasmids with T4 DNA ligase (New England Biolabs). Transfection of IHGE cells was performed using FuGENE 6 Transfection Reagent (Promega).

Immunoblotting

Immunoblotting was performed as described previously [10]. IHGE cells were lysed, and the lysates were cleared by centrifugation. Proteins were separated by SDS-PAGE and transferred to nitrocellulose membranes (0.2 μm, Bio-Rad). Membranes were blocked for 1 h at room temperature with PBST (PBS and 0.1% (v/v) Tween 20) containing 3% (w/v) skim milk, and then incubated for 1 h at room temperature with primary antibodies diluted in PBST. Next, the membranes were washed three times with PBST and incubated for 1 h at room temperature with 1:5000 dilutions of HRP-conjugated secondary antibodies in PBST. Immunoreactive bands were detected using the Pierce ECL Western Blotting Substrate (Thermo Scientific) and ChemiDoc XRS (Bio-Rad). Images were acquired using the Quantity One software (Bio-Rad).

Immunocytochemistry

Immunocytochemistry was performed as described previously [10]. IHGE cells were fixed with 4% (v/v) paraformaldehyde in PBS (Wako) overnight at room temperature, permeabilized with 0.1% (v/v) Triton X-100 (Wako) in PBS for 5 min at room temperature, and blocked with 0.1% (w/v) gelatin (Wako) in PBS for 20 min at room temperature. Samples were incubated for 1 h at room temperature with the indicated primary antibodies, washed four times in PBS, incubated for 1 h at room temperature with the Alexa Fluor–conjugated secondary antibodies (Invitrogen), and again washed four

426 times in PBS. All antibodies were diluted 1:400 in PBS. Cells were mounted onto
427 glass slides with Vectashield Mounting medium (Vector Laboratories). Images were
428 acquired with a confocal laser microscope (TCS SP8; Leica Microsystems) using a 64×
429 oil-immersion object lens with a numerical aperture of 1.4. Acquired images were
430 analyzed using the Application Suite X software (Leica Microsystems).
431
432 **Generation of cell line stably expressing CXADR**
433 Plasmid encoding CXADR was constructed by cloning PCR products amplified from the
434 pCMV plasmid into pMRX-IRES-Puro (kindly provided by Nobumichi Furuta, Osaka
435 University). Plasmids pMRX-IRES-Puro-CXADR was used for overexpression of the
436 cDNA in IHGE cells. IHGE cells were transfected with the overexpression plasmid
437 using FuGENE 6 (Promega). Seventy-two hours after transfection, cells stably
438 overexpressing the cDNA were selected with puromycin (2 μg mL^{-1}; InvivoGen).
439
440 **RNA interference**
441 Plasmid encoding shRNA was constructed by ligation of linear DNA (Sigma-Aldrich)
442 into pSIREN-RetroQ (631526, Clontech) or pSINsi-hU6 (3661, Takara). Plasmids
443 pSIREN-RetroQ-shJAM1 #110 (target sequences: 5'-
444 AAGTCAGAATTCCTGAGAATAAT-3') and #508 (target sequences: 5'-
445 GGGATAGTGATGCCTACGAATCC-3'), pSINsi-hU6-shJAM1 #508 (Fig. 9),
446 shCXADR #38 (target sequences: 5'-TAGTGGATTTCGCCAGAAGTTTG-3') and #317
447 (target sequences: 5'-ATGTAACGAATTTACAACTGTCA-3'), and shCLMP #661
448 (target sequences: 5'-GTGCGAGTAACTGTACAGTATGT-3') and #771 (target
449 sequences: 5'-AAGGAAAGACAAAGAAAGATATG-3') were used for generation of

450 the siRNA duplex in cells. Plasmid pSIREN-RetroQ-shLuc was produced as described
451 previously [10]. IHGE cells were transfected with the shRNA-encoding plasmid using
452 FuGENE 6 (Promega). Seventy-two hours after transfection, cells stably expressing the
453 shRNA were selected with puromycin (2 μg mL^{-1}) and neomycin (200 μg mL^{-1};
454 Invivogen)
455
456 **Preparation of FITC-labeled tracer**
457 Preparation of FITC-labeled tracer was performed as described previously [10]. *P.*
458 *gingivalis* LPS (14F18-MM) was purchased from Invivogen. *P. gingivalis* PGN was
459 prepared as described previously [27]. FITC–*E. coli* LPS (L7018) and *S. aureus* PGN
460 (77140) were purchased from Sigma-Aldrich. Bacterial LPS and PGN were labeled
461 with FITC using Fluorescein Labeling Kit-NH2 (LK-01, Dojindo). To generate
462 dissociated LPS and PGN, FITC-labeled LPS was diluted by 10% with water and
463 incubated with 10 mM citrate (Wako) and 0.05% (v/v) Tween-20 (Calbiochem) for 45
464 min at 37°C as described previously [28], and FITC-labeled PGN was diluted by 10%
465 with water and incubated with 0.5 mg mL^{-1} lysozyme (Nacalai Tesque) for 45 min at 37°C
466 to make a suspension. 40 kDa FITC-dextran (FD40, Sigma-Aldrich) were diluted by
467 2% with water for the permeability assay.
468
469 **Epithelial barrier function assay**
470 Epithelial barrier function assay was performed as described previously [10]. The *in*
471 *vitro* epithelial permeability assay to assess barrier function was performed with 12-well
472 cell culture inserts (353180; Corning). When IHGE cells in the upper compartment
473 reached 100% confluence, 20 μL of FITC-dextran, FITC-LPS, or FITC-PGN was added

to the upper compartment of the insert. After a 30-min incubation, the medium was collected from the lower compartment, and the fluorescence intensity was measured using 1420 ARVO *X* (PerkinElmer). Data were acquired using the WorkOut Plus software (PerkinElmer).

Statistical analysis

p-values were determined by *t* test in Excel (Microsoft); $p<0.05$ was considered significant.

Acknowledgements

We thank the Center for Oral Science, Graduate School of Dentistry, Osaka University for technical support with confocal laser microscopy. This research was supported by Grants-in-Aid for Young Scientists (B), Grant Numbers 17K17083 (to H.T.) and Scientific Research (C), Grant Numbers 19K10085 (to H.T.), and Scientific Research (A), Grant Numbers 18H04068 (to A.A.), from the Japan Society for the Promotion of Science. The funders had no role in study design, data collection, decision to publish, or preparation of the manuscript.

Author Contributions

H.T. and A.A. conceived and designed the experiments. H.T. and S.Y. performed the experiments. H.T. and A.A. analyzed the data. H.T., N.S., M.K., and M.M. contributed reagents, materials, and analytical tools. H.T. and A.A. wrote the paper.

Competing Interests

The authors have no competing financial interests to declare.

References

1. Eke, P. I., Dye, B. A., Wei, I., Thornton-Evans, G. O. & Genco, R. J. Prevalence of periodontitis in adults in the United States: 2009 and 2010. *J Dent Res.* **91**, 914-920 (2009).

2. Dixon, D. R., Bainbridge, B. W. & Darveau, R. P. Modulation of the innate response within the periodontium. *Periodontol 2000.* **35**, 53-74, (2004).

3. Kawai, T. & Akira, S. Toll-like receptors and their crosstalk with other innate receptors in infection and immunity. *Immunity.* **34**, 637-650 (2001).

4. Belibasakis, G. N., Kast, J. I., Thurnheer, T., Akdis, C. A. & Bostanci, N. The expression of gingival epithelial junctions in response to subgingival biofilms. *Virulence.* **6**, 704-709 (2005).

5. Tsukita, S., Furuse, M. & Itoh, M. Multifunctional strands in tight junctions. *Nat Rev Mol Cell Biol.* **2**, 285-293 (2001).

6. Ebnet, K., Suzuki, A., Ohno, S. & Vestweber, D. Junctional adhesion molecules (JAMs): more molecules with dual functions? *J Cell Sci.* **117**, 19-29 (2004).

7. Lamont, R. J., Koo, H. & Hajishengallis, G. The oral microbiota: dynamic communities and host interactions. *Nat Rev Microl.* **16**, 745-759 (2018).

8. Potempa, J., Pike, R. & Travis, J. The multiple forms of trypsin-like activity present in various strains of *Porphyromonas gingivalis* are due to the presence of either Arg-gingipain or Lys-gingipain. *Infect Immun.* **63**, 1176-1182 (1995).

9. Nakayama, K., Kadowaki, T., Okamoto, K. & Yamamoto, K. Construction and characterization of arginine-specific cysteine proteinase (Arg-gingipain)-deficient mutants of *Porphyromonas gingivalis*. Evidence for significant contribution of Arg-

gingipain to virulence. *J Biol Chem.* **270**, 23619-23626 (1995).

10. Takeuchi, H., Sasaki, N., Yamaga, S., Kuboniwa, M. & Amano, A. *Porphyromonas gingivalis* induces penetration of lipopolysaccharide and peptidoglycan through the gingival epithelium via degradation of junctional adhesion molecule 1. *PLoS Pathog.* **15**, e1008124; 10.1371/journal.ppat.1008124 (2019).

11. Nishiguchi, A., Yoshida, H., Matsusaki, M. & Akashi, M. Rapid construction of three-dimensional multilayered tissues with endothelial tube network by the cell-accumulation technique. *Adv Mater.* **23**, 3506-3510 (2011).

12. Bergelson, J. M. *et al*. Isolation of a common receptor for coxsackie B virus and adenoviruses 2 and 5. *Science* **275**,1320-1323 (1997).

13. Tomko, R.P., Xu, R. & Philipson, L. HCAR and MCAR: the human and mouse cellular receptors for subgroup C adenoviruses and group B coxsackieviruses. *Proc. Natl. Acad. Sci USA.* **94**, 3352-3356 (1997).

14. Watanabe, T. *et al*. Complete genome sequence of the bacterium *Porphyromonas gingivalis* TDC60, which causes periodontal disease. *J Bacteriol.* **193**, 4259-4260 (2011).

15. Kolenbrander, P. E. *et al*. Communication among oral bacteria. *Microbiol Mol Biol Rev.* **66**, 486-505 (2002).

16. Cohen, C. J. *et al*. The coxsackievirus and adenovirus receptor is a transmembrane component of the tight junction. *Proc Natl Acad Sci U S A.* **98**, 15191-15196 (2001).

17. Socransky, S. S., Haffajee, A. D., Cugini, M. A., Smith, C. & Kent, R. L. Jr. Microbial complexes in subgingival plaque. *J Clin Periodontol.* **25**, 134-144 (1998).

18. Ishihara, K., Miura, T., Kuramitsu, H. K. & Okuda, K. Characterization of the *Treponema denticola* prtP gene encoding a prolyl-phenylalanine-specific protease

563 (dentilisin). *Infect Immun.* **64**: 5178-5186 (1996).
564
565 19. Fenno, J. C., Lee, S. Y., Bayer, C. H. & Ning Y. The opdB locus encodes the trypsin-
566 like peptidase activity of *Treponemma denticola*. *Infect Immun.* **69**, 6193-6200 (2001).
567
568 20. Nakajima, T. *et al*. Isolation and identification of a cytopathic activity in *Tannerella*
569 *forsythia*. *Biochem Biophys Res Commun.* **351**, 133-139 (2006).
570
571 21. Patzke, C. *et al*. The coxsackievirus-adenovirus receptor reveals complex homophilic
572 and heterophilic interactions on neural cells. *J Neurosci.* **30**, 2897-2910 (2010).
573
574 22. Mandell, K. J., McCall, I. C. & Parkos, C. A. Involvement of the junctional adhesion
575 molecule-1 (JAM1) homodimer interface in regulation of epithelial barrier function. *J*
576 *Biol Chem.* **279**, 16254-16262 (2004).
577
578 23. Azari, B. M. *et al*. Transcription and translation of human F11R gene are required for
579 an initial step of atherogenesis induced by inflammatory cytokines. *J Transl Med.* **9**, 98;
580 10.1186/1479-5876-9-98 (2011).
581
582 24. Chung, J. *et al*. Coxsackievirus and adenovirus receptor mediates the responses of
583 endothelial cells to fluid shear stress. *Exp Mol Med.* **51**, 1-15 (2019).
584
585 25. Shi, Y. *et al*. Genetic analysis of proteolysis, hemoglobin binding, and
586 hemagglutination of *Porphyromonas gingivalis*. Construction of mutants with a
587 combination of rgpA, rgpB, kgp, and hagA. *J Biol Chem.* **274**, 17955-17960 (1999).
588
589 26. Murakami, S. *et al*. Activation of adenosine-receptor-enhanced iNOS mRNA
590 expression by gingival epithelial cells. *J Dent Res.* **81**, 236-240 (2002).
591
592 27. Ishii, K. *et al*. *Porphyromonas gingivalis* peptidoglycans induce excessive activation
593 of the innate immune system in silkworm larvae. *J Biol Chem.* **285**, 33338-33347 (2010).
594

28. Reich, J., Lang, P., Grallert, H. & Motschmann, H. Masking of endotoxin in surfactant samples: Effects on Limulus-based detection systems. *Biologicals.* **44**, 417-422 (2016).

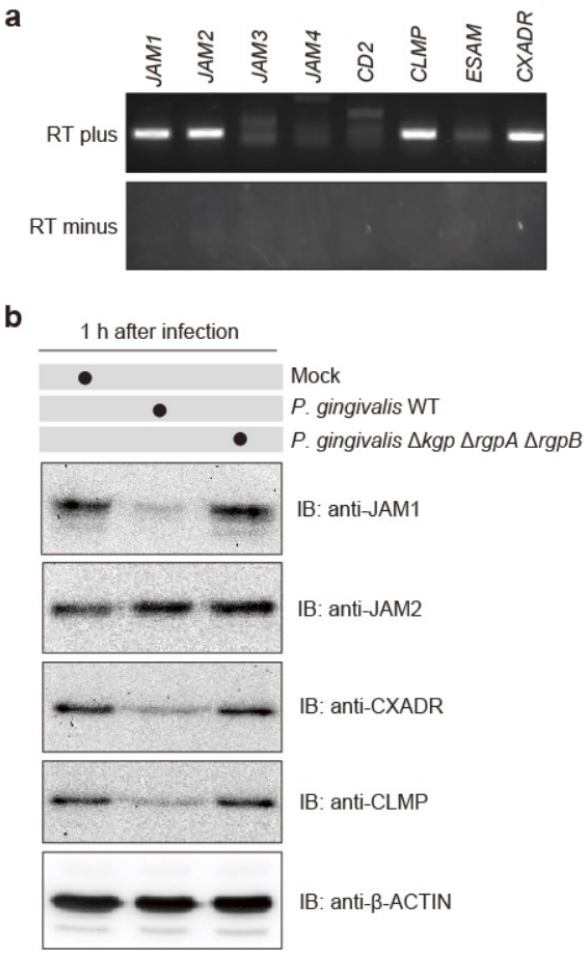

599

600

601 **Figure 1.** ***P. gingivalis*** **gingipains degrade CXADR in IHGE cells.**

602 **(a)** Expression of *JAM1*, *JAM2*, *JAM3*, *JAM4*, *CD2*, *CLMP*, *ESAM*, and *CXADR* by IHGE

603 cells analyzed by RT-PCR. **(b)** IHGE cells were infected with *P. gingivalis* WT or Δ*kgp*

604 Δ*rgpA* Δ*rgpB* mutant at an MOI of 100 for 1 h. The cells were then analyzed by

605 immunoblotting with the indicated antibodies. β-ACTIN was used as a loading control.

606 RT, reverse transcription. IB, immunoblot.

607

608

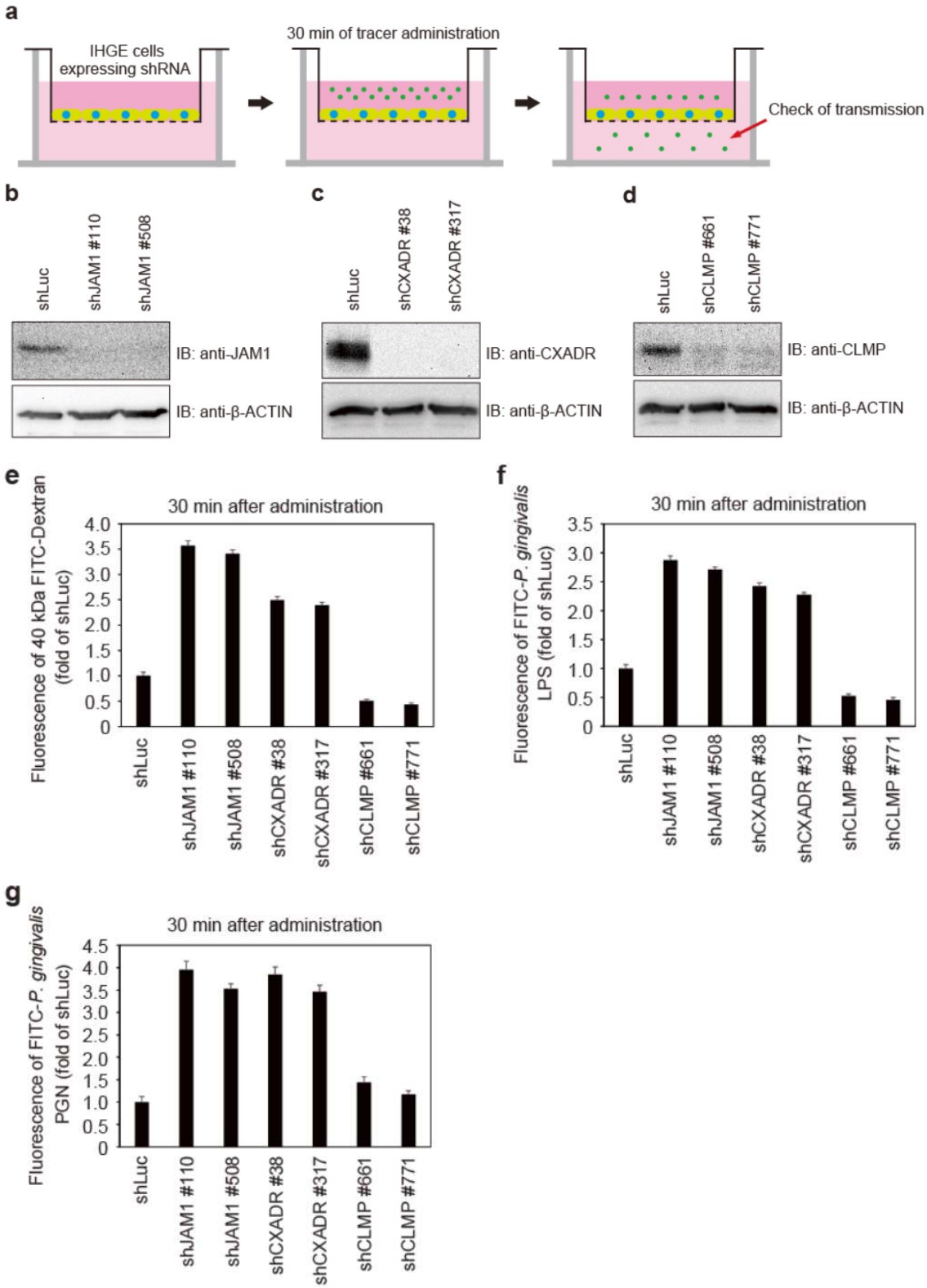

609

610

611 **Figure 2. Loss of CXADR increased the epithelial barrier permeability.**

(a) Schematic image of the culture insert system. Monolayer of IHGE cells stably expressing shLuc, shJAM1 #110, shJAM1 #508, shCXADR #38, shCXADR #317, shCLMP #661, and shCLMP #771 were cultured in culture inserts. FITC-labeled tracer was added to culture media in the upper compartment. Following 30 min of incubation, the transmission of tracer from the upper compartment to the lower compartment was analyzed by spectrometry. **(b-d)** IHGE cells stably expressing shLuc, shJAM1, shCXADR, or shCLMP were analyzed by immunoblotting with the indicated antibodies. **(e-f)** Permeability to 40 kDa FITC-dextran (e), FITC–*P. gingivalis* LPS (f), FITC–*P. gingivalis* PGN (g) in IHGE cells expressing indicated shRNA. Results are expressed as fold change relative to cells expressing shLuc and are the means ± SD of eight technical replicates.

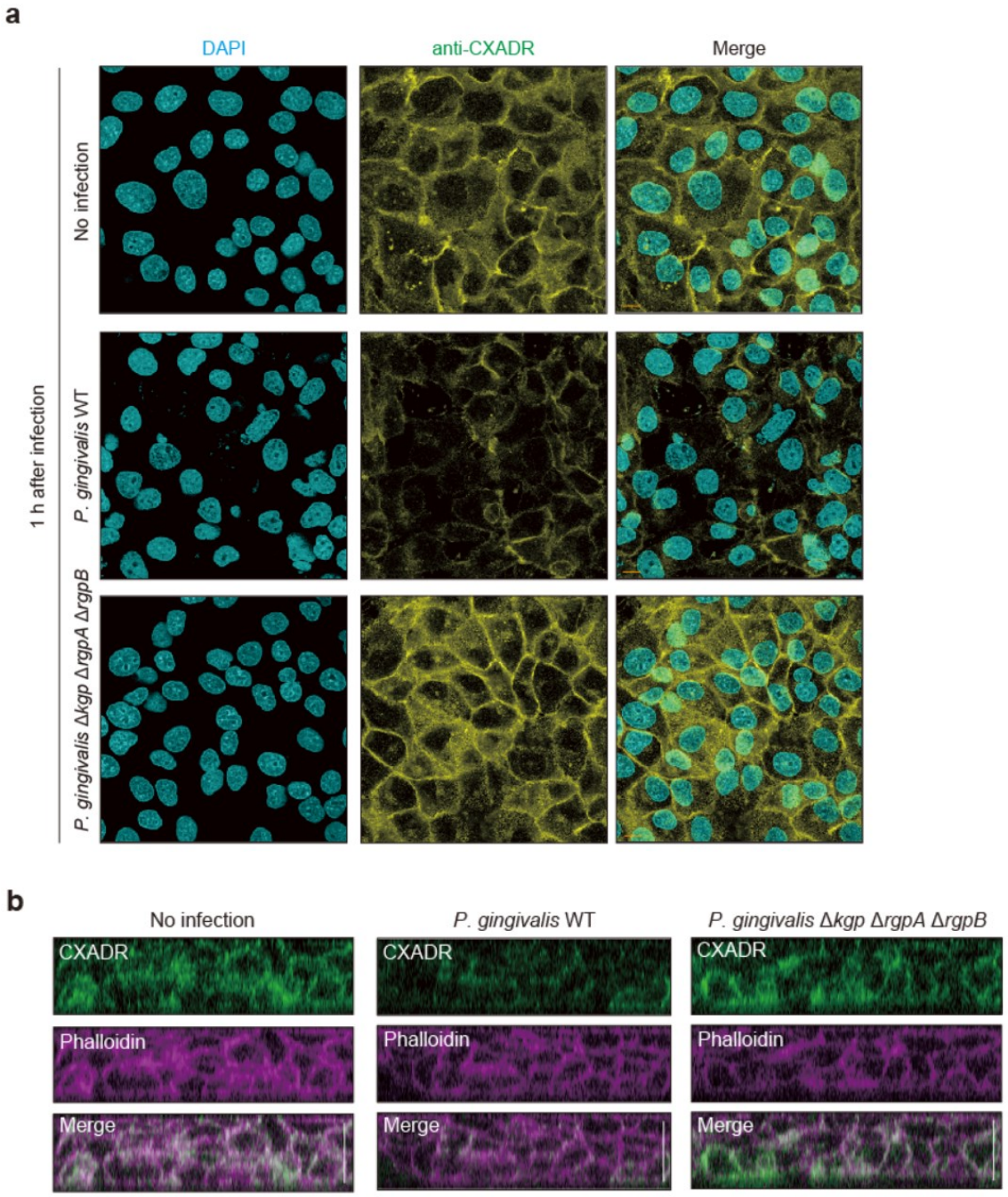

626

627

628

629 **Figure 3. Degradation of CXADR in IHGE cells infected with *P. gingivalis***

630 **gingipains**

631 **(a)** IHGE cells were infected with *P. gingivalis* WT or Δ*kgp* Δ*rgpA* Δ*rgpB* mutant at an

632 MOI of 100 for 1 h. The cells were then fixed, stained with DAPI (cyan) and anti-

633 CXADR (yellow), and analyzed by confocal microscopy. Scale bars, 10 μm. **(b)**
634 Gingival epithelial tissues on coverslips were infected with *P. gingivalis* WT or Δ*kgp*
635 Δ*rgpA* Δ*rgpB* mutant for 2 h. The tissues were then fixed, stained with anti-CXADR
636 (green) and Alexa Fluor 568–conjugated phalloidin (magenta), and analyzed by confocal
637 microscopy. Scale bars, 30 μm.
638
639
640

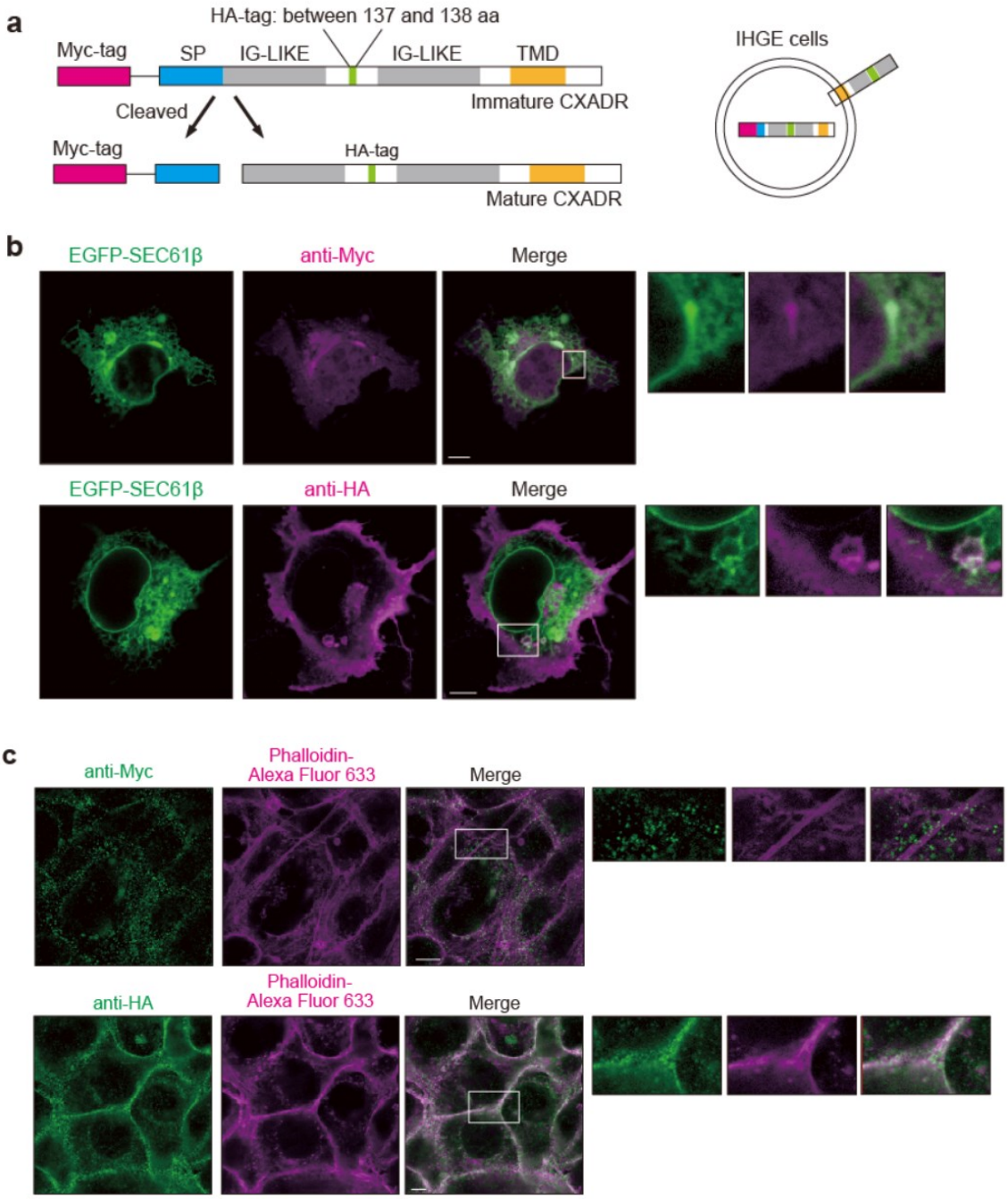

641

642

643

644 **Figure 4. Localization of CXADR in IHGE cells.**

645 **(a)** Schematic view of the structure of Myc–tagged HA–inserted CXADR. Immature
646 form of Myc–tagged HA–inserted CXADR was used as an internal control to monitor
647 degradation flux of mature form of HA-inserted CXADR. The Myc tag is indicated by

the magenta box, and the HA-tag is indicated by the green box. The signal peptide is indicated by the blue box, and IG-LIKE or TMD domains are indicated by gray boxes or an orange box, respectively. **(b,c)** IHGE cells were transiently transfected with plasmids encoding Myc–tagged HA–inserted CXADR; in (b), the cells were also transfected with EGFP-SEC61β (green). Following 48 h of incubation, cells were fixed, stained with anti-Myc (b, magenta; c, green) or anti-HA (b, magenta; c, green): in (c), the cells were also stained with Alexa Fluor 633–conjugated phalloidin (magenta). The cells were then analyzed by immunofluorescence microscopy. Higher magnification of the areas indicated by white boxes in the upper panels are shown in the right side. Scale bars, 5 μm.

660

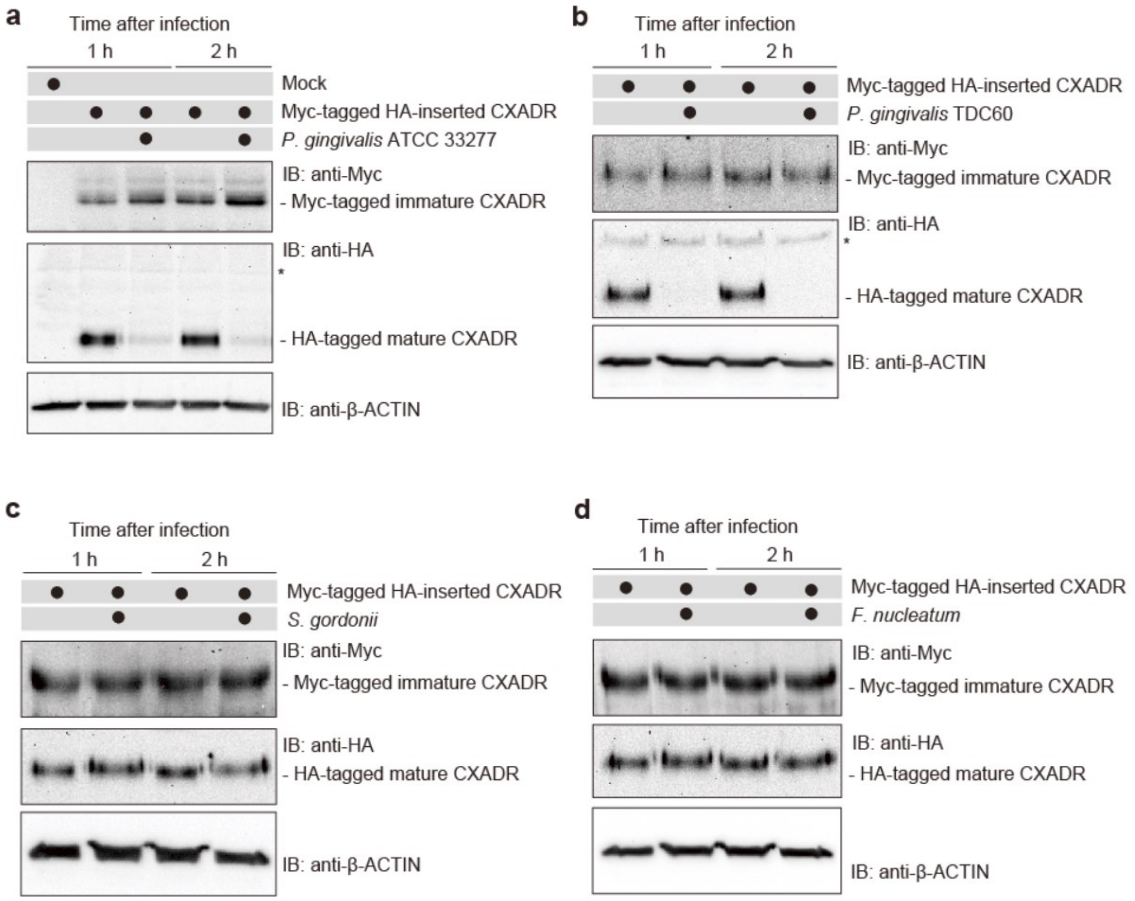

661

662

663 **Figure 5.** ***P. gingivalis*****, but not** ***S. gordonii*** **or** ***F. nucleatum*****, degrades CXADR in**

664 **IHGE cells.**

665 **(a–d)** IHGE cells were transiently transfected with Myc–tagged HA–inserted CXADR

666 plasmid. Following 48 h of incubation, the cells were infected with *P. gingivalis* ATCC

667 33277 (a), *P. gingivalis* TDC60 (b), *S. gordonii* DL-1 (c), or *F. nucleatum* ATCC 25586

668 (d) at an MOI of 100 for the indicated times. The cells were then analyzed by

669 immunoblotting with the indicated antibodies.

670

671

672

673

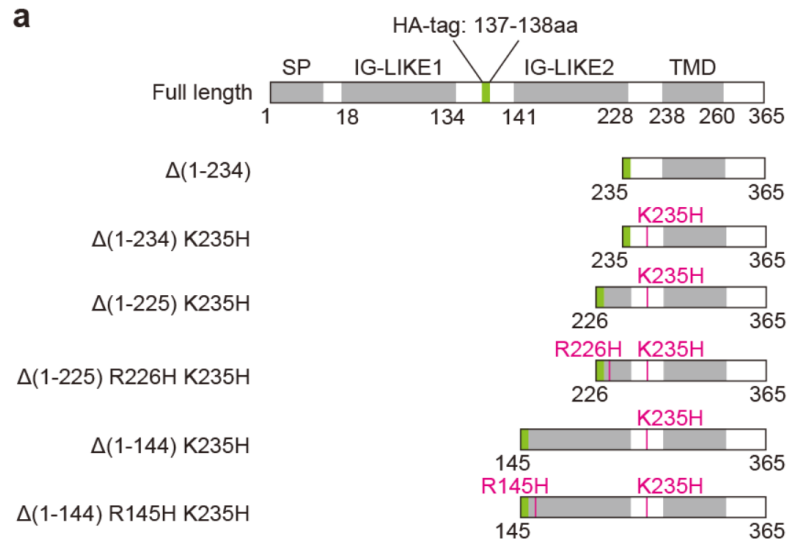

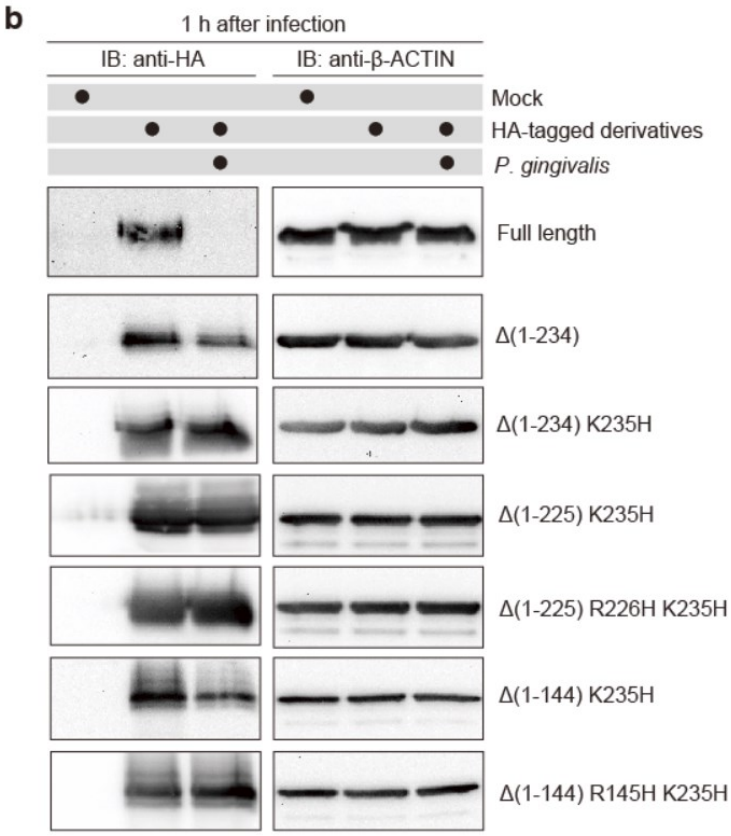

674

675

676 **Figure 6. The R145 and K235 residues are targeted for degradation of CXADR by**

677 ***P. gingivalis* in IHGE cells**

678 **(a)** Schematic view of the CXADR structure and derivatives. SP, IG-LIKE, or TMD

679 domains are indicated by gray boxes. HA-tag is shown in green. The point mutations
680 R145H and K235H are shown in magenta. **(b)** IHGE cells were transiently transfected
681 with plasmid encoding HA–inserted CXADR or the indicated CXADR mutants.
682 Following 48 h of incubation, the cells were infected with *P. gingivalis* at an MOI of 100
683 for 1 h, and then analyzed by immunoblotting using the indicated antibodies.
684
685
686

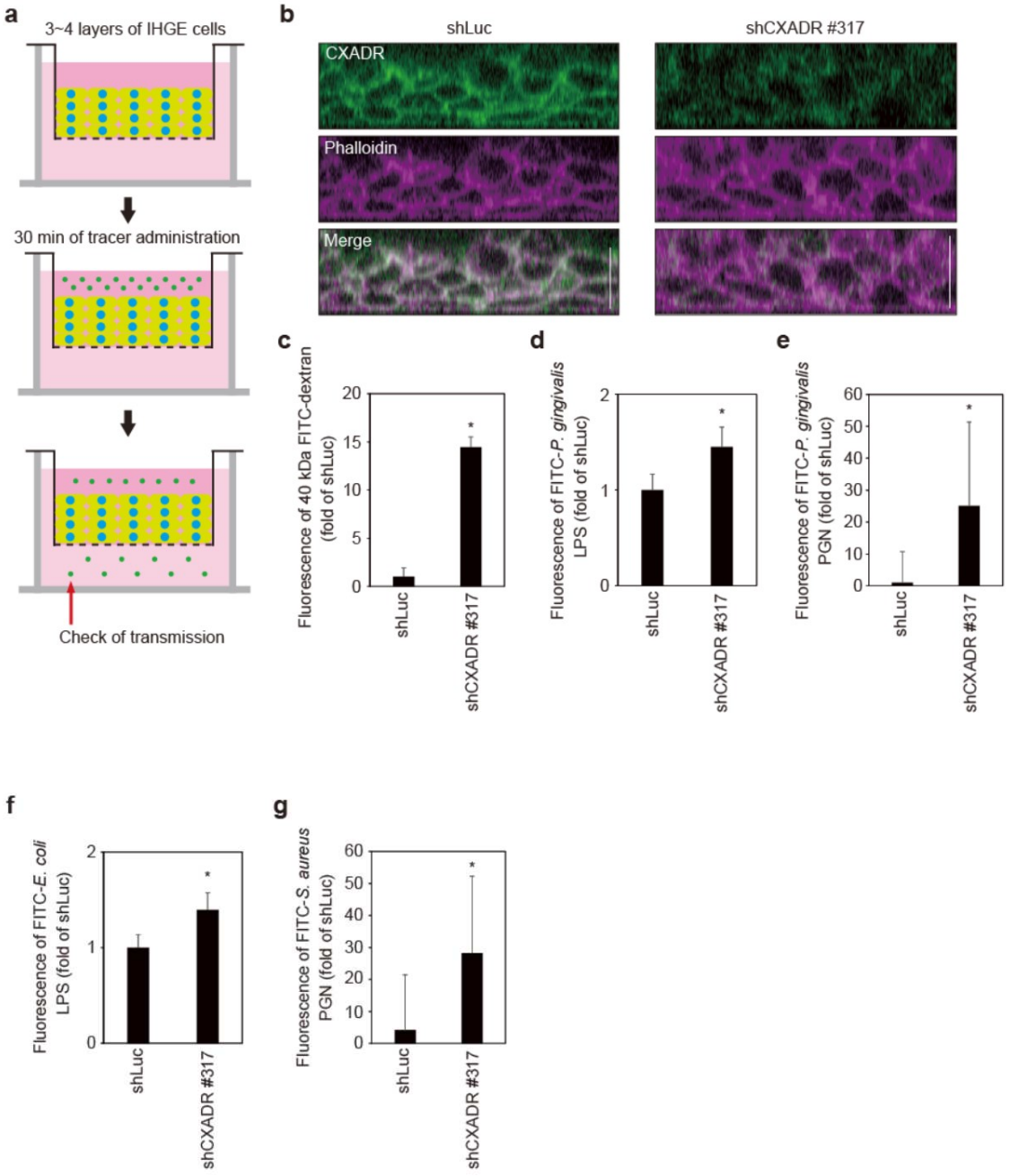

687

688

689

690 **Figure 7. CXADR is required for epithelial barrier function of gingival epithelial**

691 **tissues.**

692 **(a,b)** Schematic illustration (a) and confocal microscopic cross-sectional images (b) of

693 3D-tissue model expressing shLuc or shCXADR. Gingival epithelial tissues were fixed,

694 stained with anti-CXADR (green) and Alexa Fluor 568–conjugated phalloidin (magenta),
695 and analyzed by confocal microscopy. Scale bars, 30 μm. **(c–g)** Permeability to 40
696 kDa FITC–dextran (c), FITC–*P. gingivalis* LPS (d), FITC–*P. gingivalis* PGN (e), FITC–
697 *E. coli* LPS (f), and FITC–*S. aureus* PGN (g) in gingival epithelial tissues expressing
698 shLuc and shCXADR. Results are expressed as fold change relative to epithelium
699 expressing shLuc and are the means ± SD of seven technical replicates. *, $p<0.05$, one-
700 tailed *t* test (c–e).
701

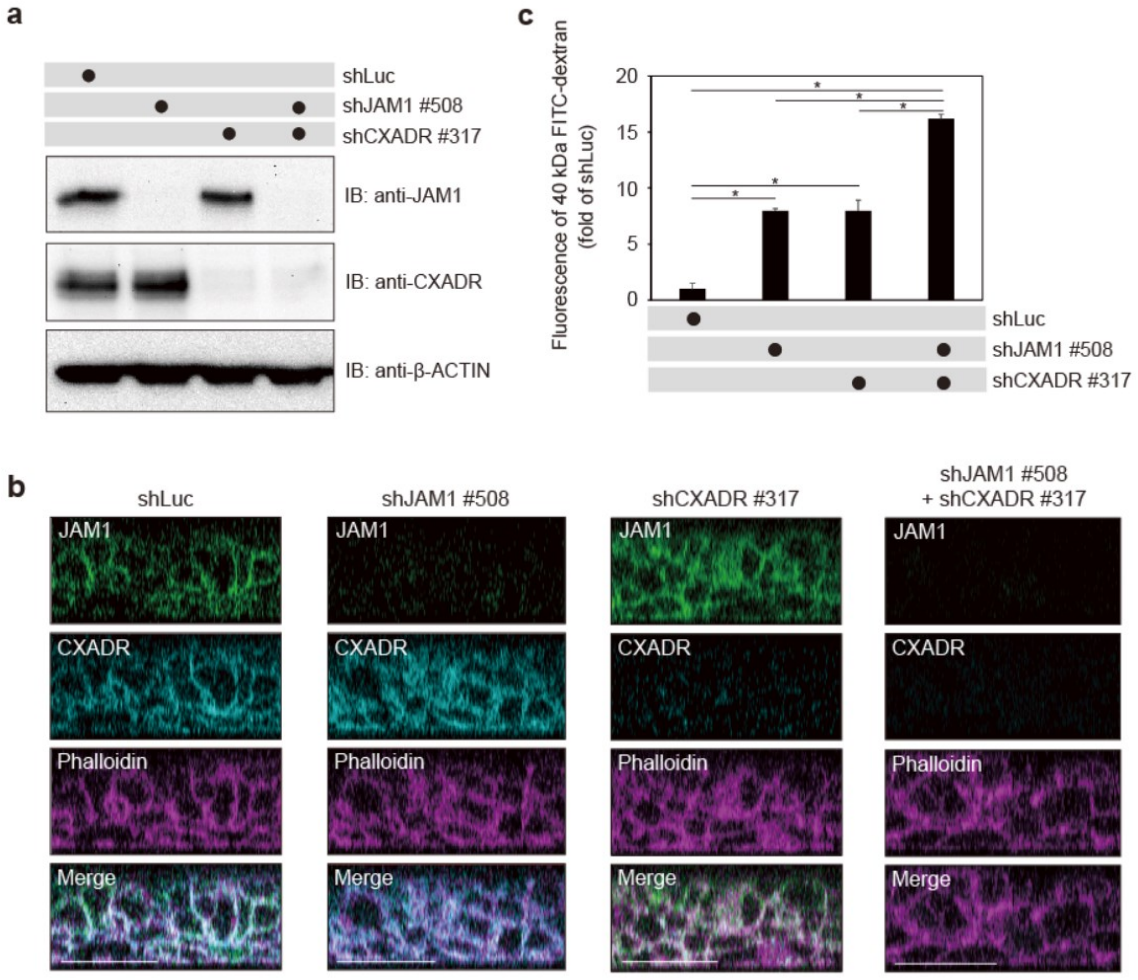

Figure 8. Barrier function in gingival epithelial tissues is regulated by CXADR independently of JAM1.

(a) IHGE cells stably expressing shLuc, shJAM1 #508, shCXADR #317, or both shJAM1 #508 and shCXADR #317 were analyzed by immunoblotting with the indicated antibodies. **(b)** Gingival epithelial tissues stably expressing shLuc, shJAM1 #508, shCXADR #317, or both shJAM1 #508 and shCXADR #317 on coverslips were fixed, stained with anti-JAM1 (green), anti-CXADR (cyan) and Alexa Fluor 568–conjugated phalloidin (magenta), and analyzed by confocal microscopy. Scale bars, 30 μm. **(c)** Permeability to 40 kDa FITC–dextran in gingival epithelial tissues expressing shLuc,

714 shJAM1 #508, shCXADR #317, or both shJAM1 #508 and shCXADR #317. Results
715 are expressed as fold change relative to epithelium expressing shLuc and are the means ±
716 SD of eight technical replicates. *, $p<0.05$, two-tailed *t* test.
717
718

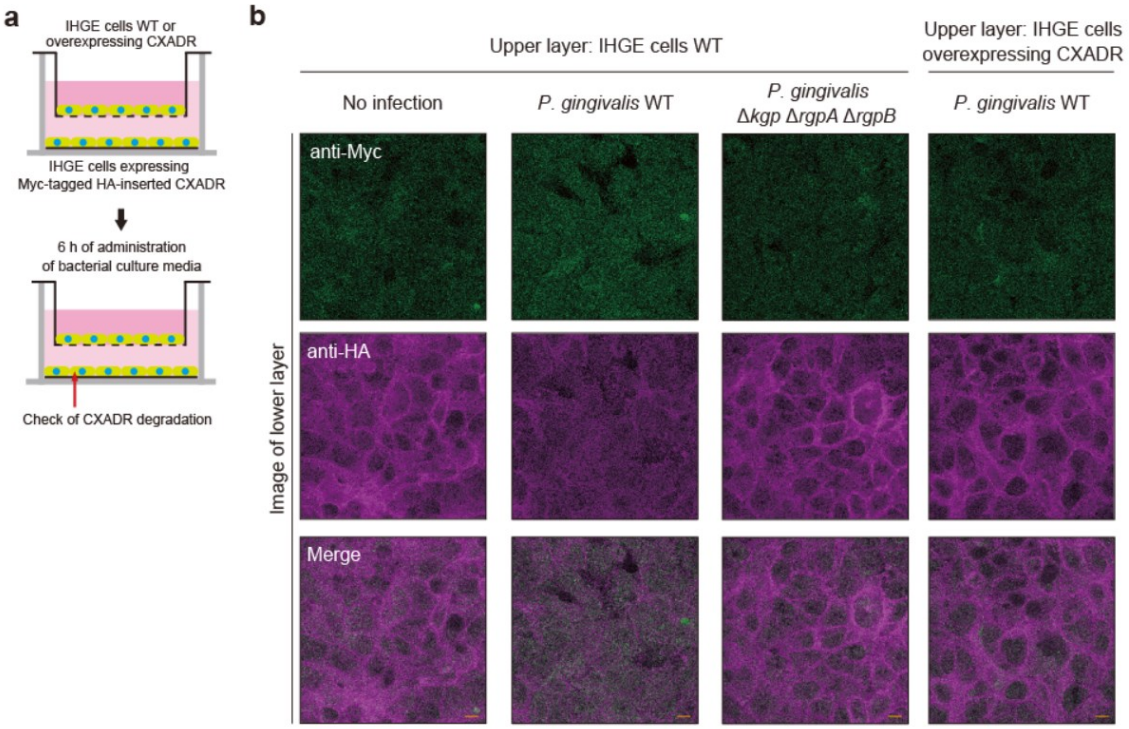

719

720

721 **Figure 9.** ***P. gingivalis*** **gingipains penetrate the epithelial barrier of IHGE cells.**

722 **(a, b)** Schematic image of the culture insert system (a). Gingival epithelial cells WT or

723 stably expressing Myc-tagged HA-inserted CXADR were cultured in the upper

724 compartment and IHGE cells stably expressing Myc-tagged HA-inserted CXADR on a

725 coverslip in the lower compartment. The bacterial culture supernatant of *P. gingivalis*

726 WT or or Δ*kgp* Δ*rgpA* Δ*rgpB* mutant was administered to cells. Following 6 h of

727 incubation, cells in the lower compartment were fixed, stained with anti-Myc (green), and

728 anti-HA (magenta), and analyzed by confocal microscopy (b). Scale bars, 10 μm.

729

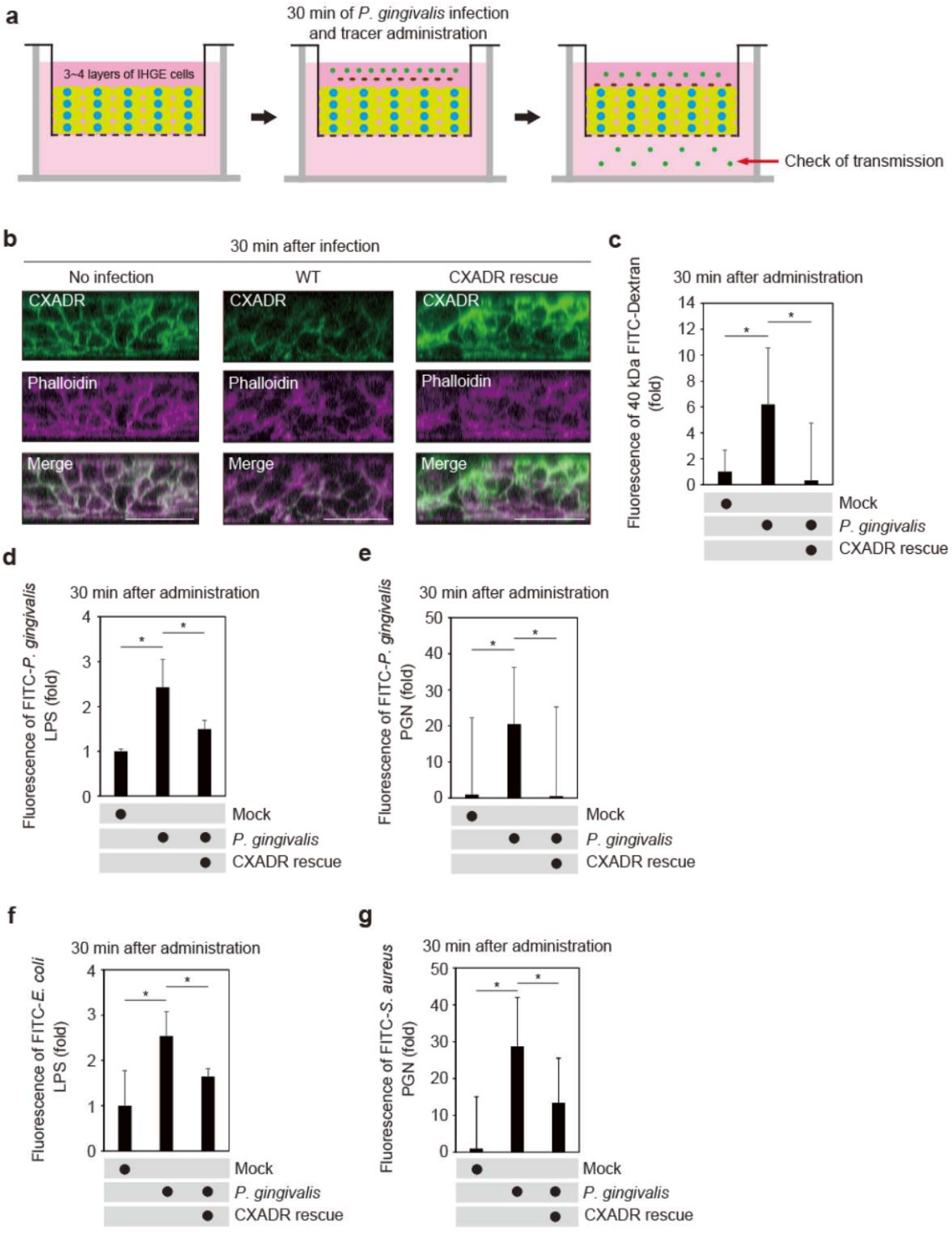

Figure 10. ***P. gingivalis*** **degrades CXADR of gingival epithelium, causing penetration of LPS and PGN.**

(a,b) Schematic illustration of the three-dimensional culture (a) and confocal microscopic

cross-sectional images (b) of the three-dimensional culture of IHGE cells. Gingival epithelial tissues (WT or overexpressing CXADR) were infected with *P. gingivalis* for 30 min. Tissues were then fixed, stained with anti-CXADR (green) and Alexa Fluor 568–conjugated phalloidin (magenta), and analyzed by confocal microscopy. Scale bars, 30 μm. **(c–g)** Permeability to 40 kDa FITC-dextran (c), FITC–*P. gingivalis* LPS (d), FITC–*P. gingivalis* PGN (e), FITC–*E. coli* LPS (f), and FITC–*S. aureus* PGN (g) of gingival epithelial tissues (WT or overexpressing CXADR) infected with *P. gingivalis*. Three-dimensional tissues on culture inserts were infected with *P. gingivalis* and FITC-labeled tracer in the upper compartment. Following 30 min of incubation, the transmission of tracer from the upper compartment to the lower compartment was analyzed by spectrometry. Results are expressed as fold change relative to uninfected WT cells and are the means ± SD of seven technical replicates. *, $p<0.05$, one-tailed *t* test (closed testing procedure).

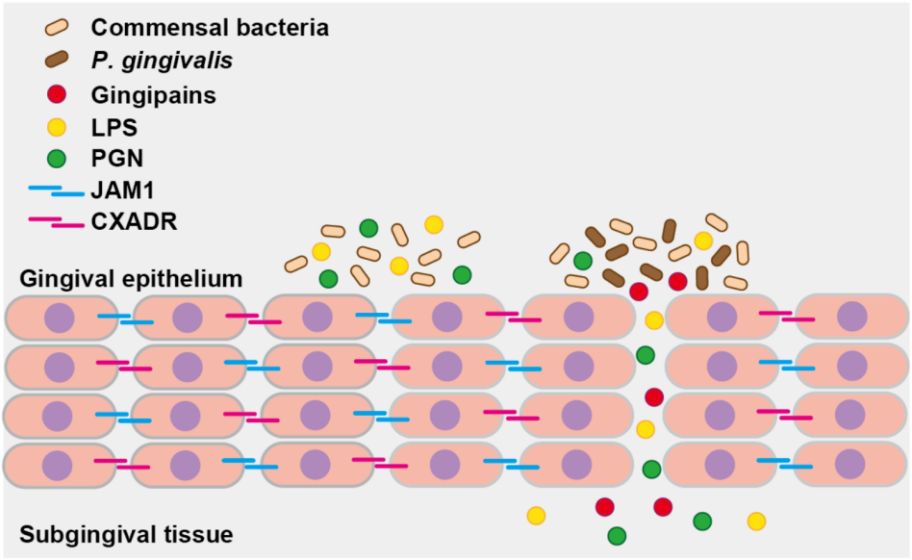

Figure 11. Proposed model of how *P. gingivalis* gingipains send bacterial virulence factors through the gingival epithelium.

In gingival epithelial tissues CXADR (magenta) and JAM1 (cyan) are not interdependent on the permeability. *P. gingivalis* gingipains degrade CXADR and JAM1, which increases the permeability of gingival epithelium to gingipains and other factors. Subsequently, gingipains are transferred to the deeper epithelium to further degrade CXADR and JAM1, which allows LPS and PGN to penetrate the gingival epithelium and reach subepithelial tissues. Finally, gingipains, LPS, and PGN induce inflammation in gingival tissues.

Figures

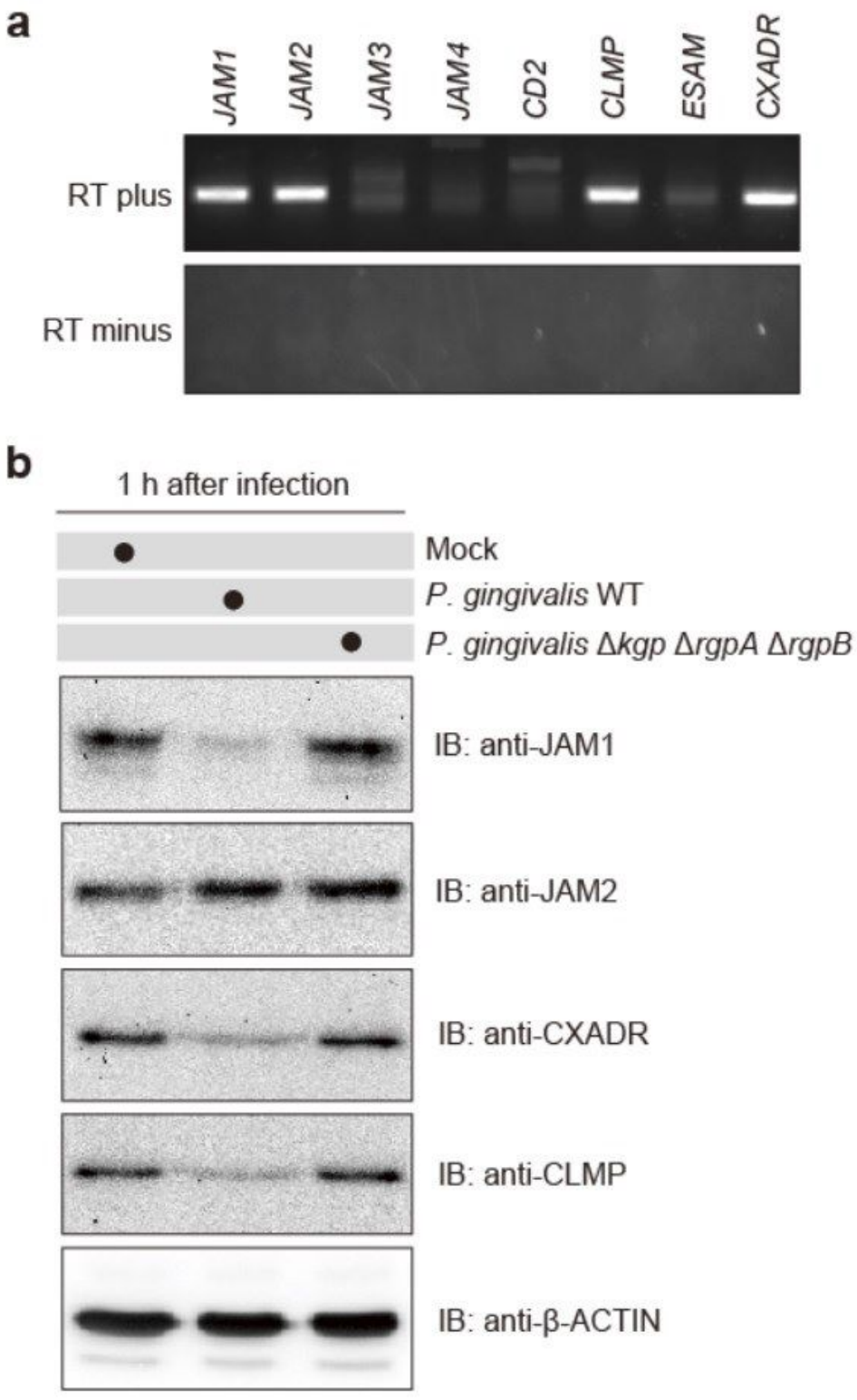

Figure 1

P. gingivalis gingipain s degrade CXADR in IHGE cells. (aExpression of JAM1 , JAM2 , JAM3 , JAM4 , CD2 , CLMP , ESAM , and CXADR by IHGE cells analyzed by RT PCR (b IHGE cells were infected with P. gingivalis WT or Δ kgp Δ rgpA Δ rgpB mutant at an MOI of 100 for 1 h. The cells were then analyzed by

immunoblotting with the indicated antibodies. β ACTIN was used as a loading control. RT, reverse transcription. IB, immunoblot.

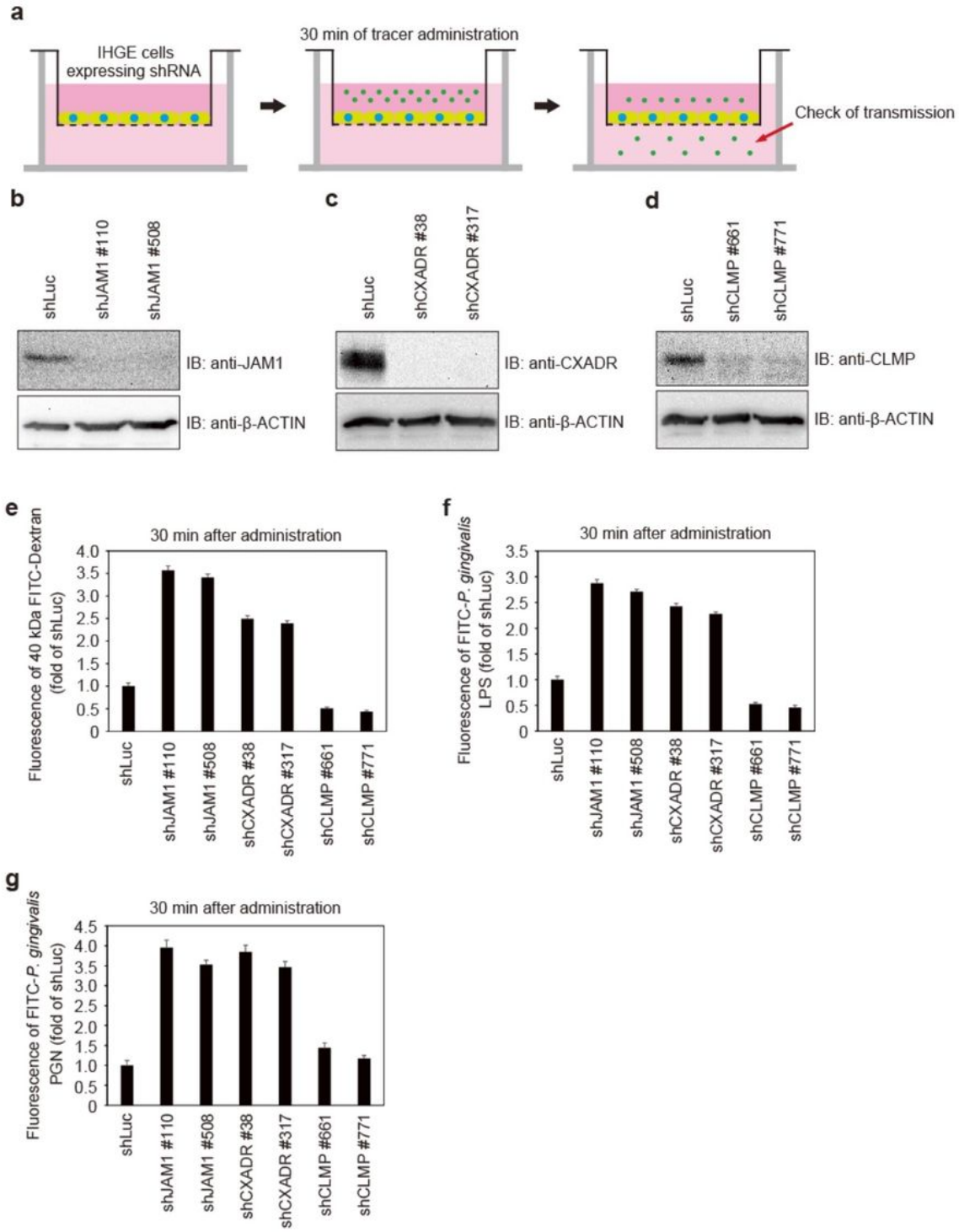

Figure 2

Loss of CXADR increased the epithelial barrier permeability. (a (a)) Schematic image of Schematic image of the culture insert system. Monolayer of IHGE cells stably the culture insert system. Monolayer of IHGE cells stably exexpressing shLuc, shJAM1 #110, pressing shLuc, shJAM1 #110, shJAM1 #508shJAM1

#508, shCXADR #38, shCXADR #317, , shCXADR #38, shCXADR #317, 613 shCLMP #661, and shCLMP #771shCLMP #661, and shCLMP #771 were cultured in culture inserts. FITCwere cultured in culture inserts. FITC–labeled tracer labeled tracer was added to culture media in the upper cowas added to culture media in the upper compartment. Following 30 min of incubation, mpartment. Following 30 min of incubation, the transmission of tracer from the upper compartment to the lower compartment was the transmission of tracer from the upper compartment to the lower compartment was analyzed by spectrometry. analyzed by spectrometry. (b(b–dd)) IHGE cells stably exIHGE cells stably expressing pressing shLuc, shJAM1, shLuc, shJAM1, shCXADR, or shCLMPshCXADR, or shCLMP werewere analyzed by immunoblotting wanalyzed by immunoblotting with the indicated antibodies. ith the indicated antibodies. (e(e–ff)) Permeability to 40 kDa FITCPermeability to 40 kDa FITC–dextran (dextran (ee)),, FITCFITC––P. gingivalisP. gingivalis LPS (LPS (ff), FITC), FITC––P. P. gingivalisgingivalis PGN (PGN (gg) in IHGE cells expressing indicated shRNA) in IHGE cells expressing indicated shRNA. Results are expressed . Results are expressed as fold change relative to cells expressing shLucas fold change relative to cells expressing shLuc and are the means ± SD of eight technical and are the means ± SD of eight technical replicates. replicates.

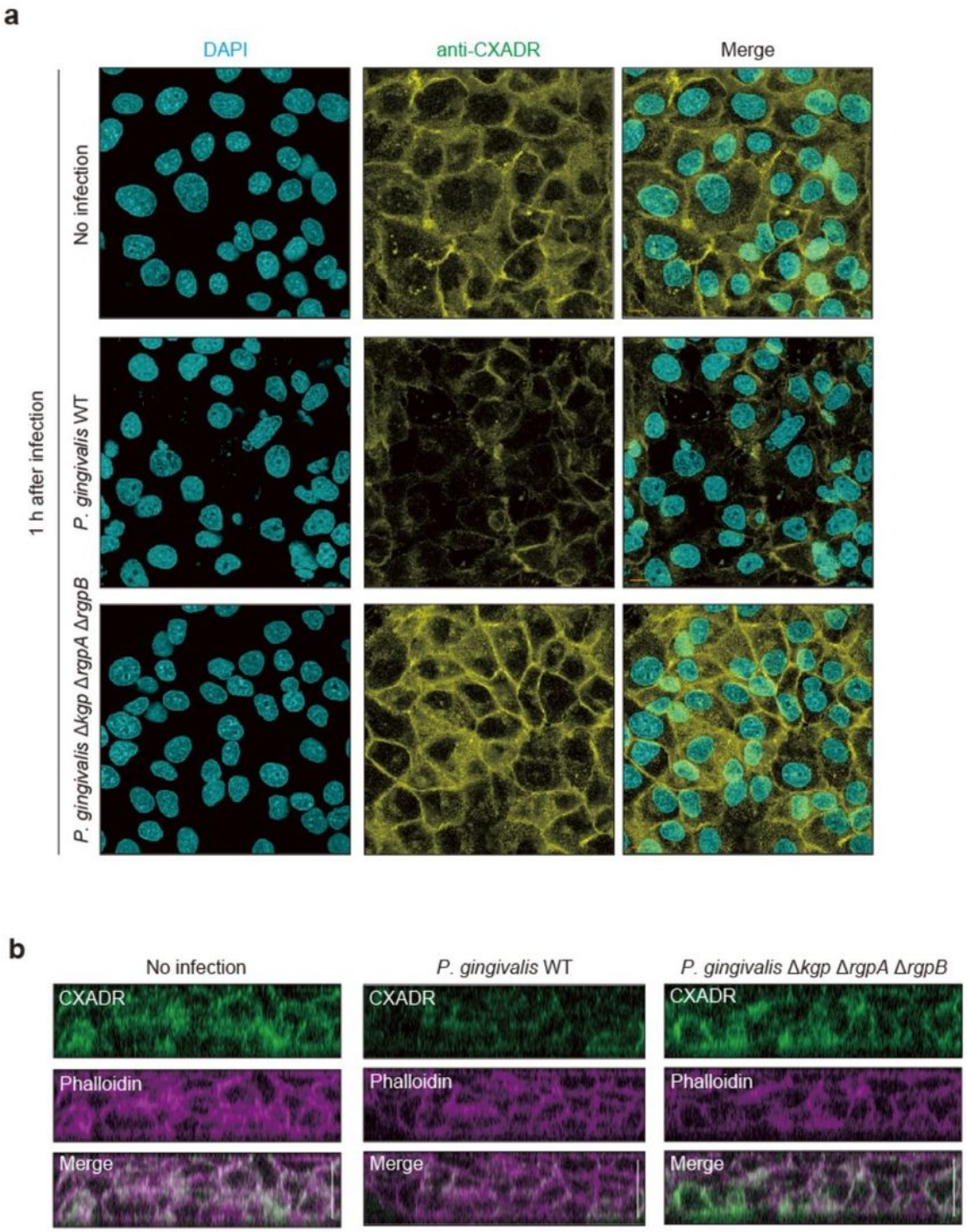

Figure 3

Degradation of CXADR in IHGE cells infected with P. gingivalis gingipains (a IHGE cells were infected with P. gingivalis WT or Δ kgp Δ rgpA Δ rgpB mutant at an MOI of 100 for 1 h. The cells were then fixed, staine d with DAPI (cyan) and anti CXADRCXADR (yellow), and analyzed by confocal microscopy. Scale bars, 10 μm. (yellow), and analyzed by confocal microscopy. Scale bars, 10 μm. ((bb)) GGingival epithelial tissues on coverslips were infected with ingival epithelial tissues on coverslips were infected with P. gingivalisP.

gingivalis WT or WT or ΔΔkgpkgp ΔΔrgpArgpA ΔΔrgpBrgpB mutantmutant for 2 h. for 2 h. The tissues The tissues were thwere then fixed, stained with antien fixed, stained with anti–CXADRCXADR 6 (green(green) and Alexa Fluor 568) and Alexa Fluor 568––conjugated phconjugated phalloidin (magenta), and analyzed by confocal alloidin (magenta), and analyzed by confocal microscopy. Scale bars, 30 μm.microscopy. Scale bars, 30 μm.

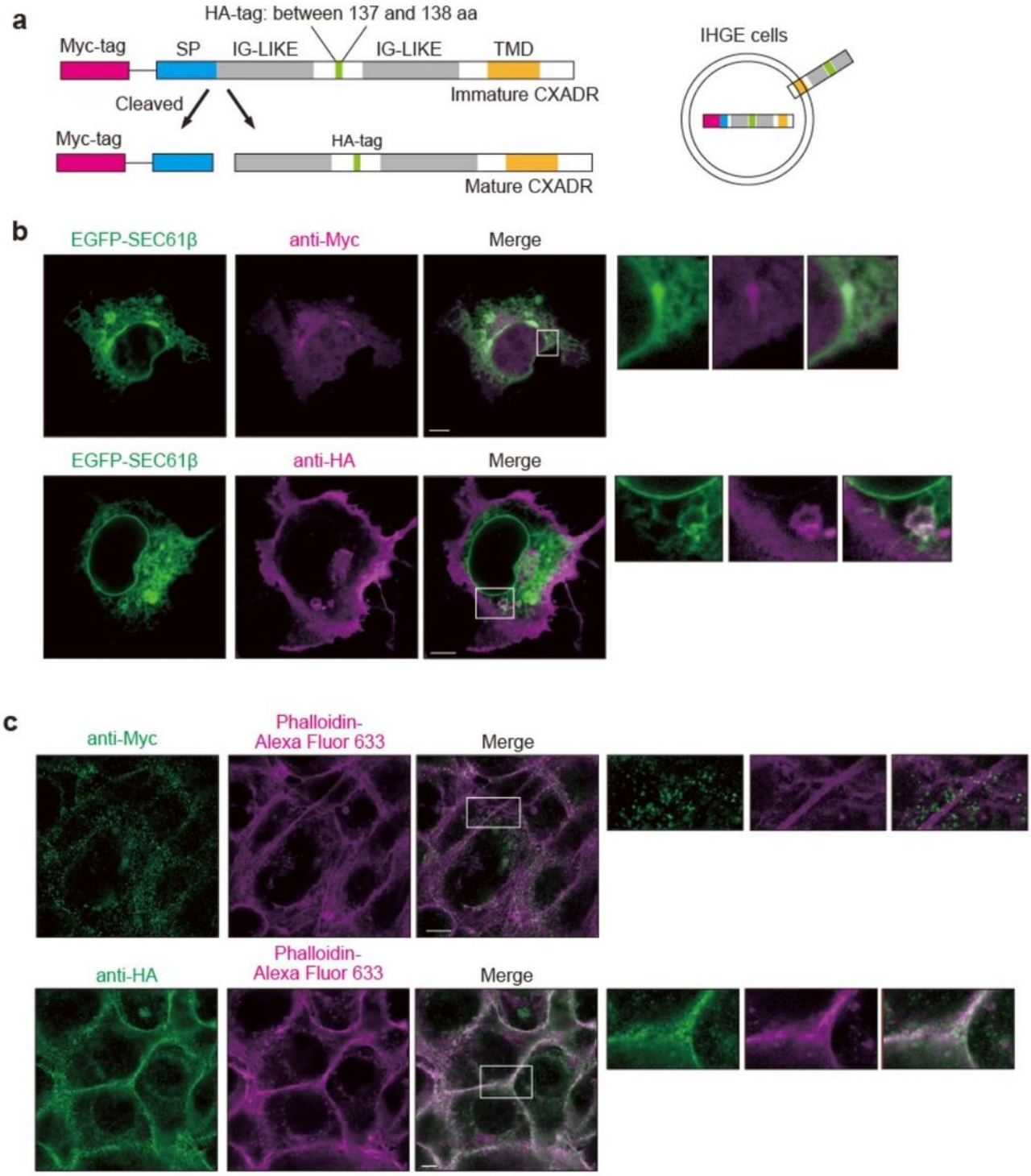

Figure 4

Localization of CXADR in IHGE cells. (aSchematic view of the structure of Myc tagged HA inserted CXADR. Immature form of Myc tagged HA inserted CXADR was used as an internal control to monitor degradation flux of mature form of HA inserted CXADR. The Myc tag is indicated by the magenta box, athe magenta box, and the HAnd the HA–tag is indicated by the green box. tag is indicated by the green box. The signal peptide is The signal peptide is indicated by the blue box, and IGindicated by the blue box, and IG–LIKE or TMD domains are indicated by gray boxes or LIKE or TMD domains are indicated by gray boxes or an orange box, respectively. an orange box, respectively. ((bb„cc)) IHGE cells were transiently transfected with plasmids IHGE cells were transiently transfected with plasmids encoding Mycencoding Myc––ttagged HAagged HA––inserted CXADR; in (inserted CXADR; in (bb), the cells were also transfected with), the cells were also transfected with EGFPEGFP–SEC61βSEC61β (green). Following 48 h of incubation, cells were(green). Following 48 h of incubation, cells were fixed, stained with fixed, stained withantianti–Myc (b, magenta; c, green) or antiMyc (b, magenta; c, green) or anti–HA (b, magenta; cHA (b, magenta; c, green), green): in (c: in (c)), , the cells werethe cells were also stained with Alexa Fluor 633also stained with Alexa Fluor 633––conjugated phalloidin (magenta).conjugated phalloidin (magenta). The cells were The cells were 654 then analyzed by immunofluorescence microscopy.then analyzed by immunofluorescence microscopy. Higher magnification of the areas Higher magnification of the areas indicated by white boxes in the upper panels are shown in the right side.indicated by white boxes in the upper panels are shown in the right side. Scale bars, 5 Scale bars, 5 μm.μm.

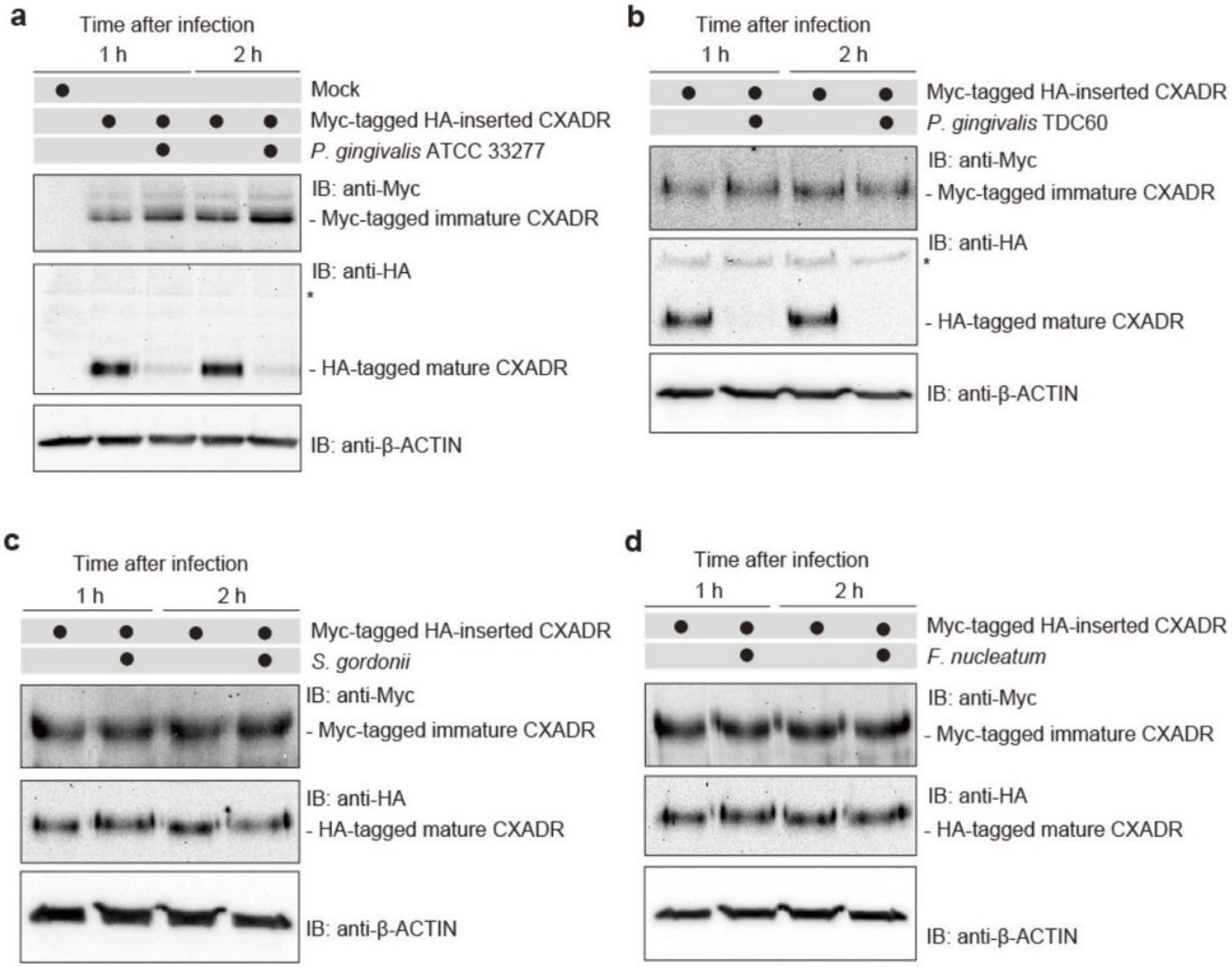

Figure 5

P. gingivalis , but not S. gordonii or F. nucleatum , degrades CXADR in 663 IHGE cells. (a d IHGE cells were transiently transfected with Myc tagged HA inserted CXADR plasmid. Following 48 h of incubation, the cells were infected with P. gingivalis ATCC 33277 (a), P. gingivalis TDC60 (b), S. gordonii DL 1 c), or F. nucleatum ATCC 25586 d) at an MOI of 100 for the indicated times. The cells were then analyzed by immunoblotting with the indicated antibodies.

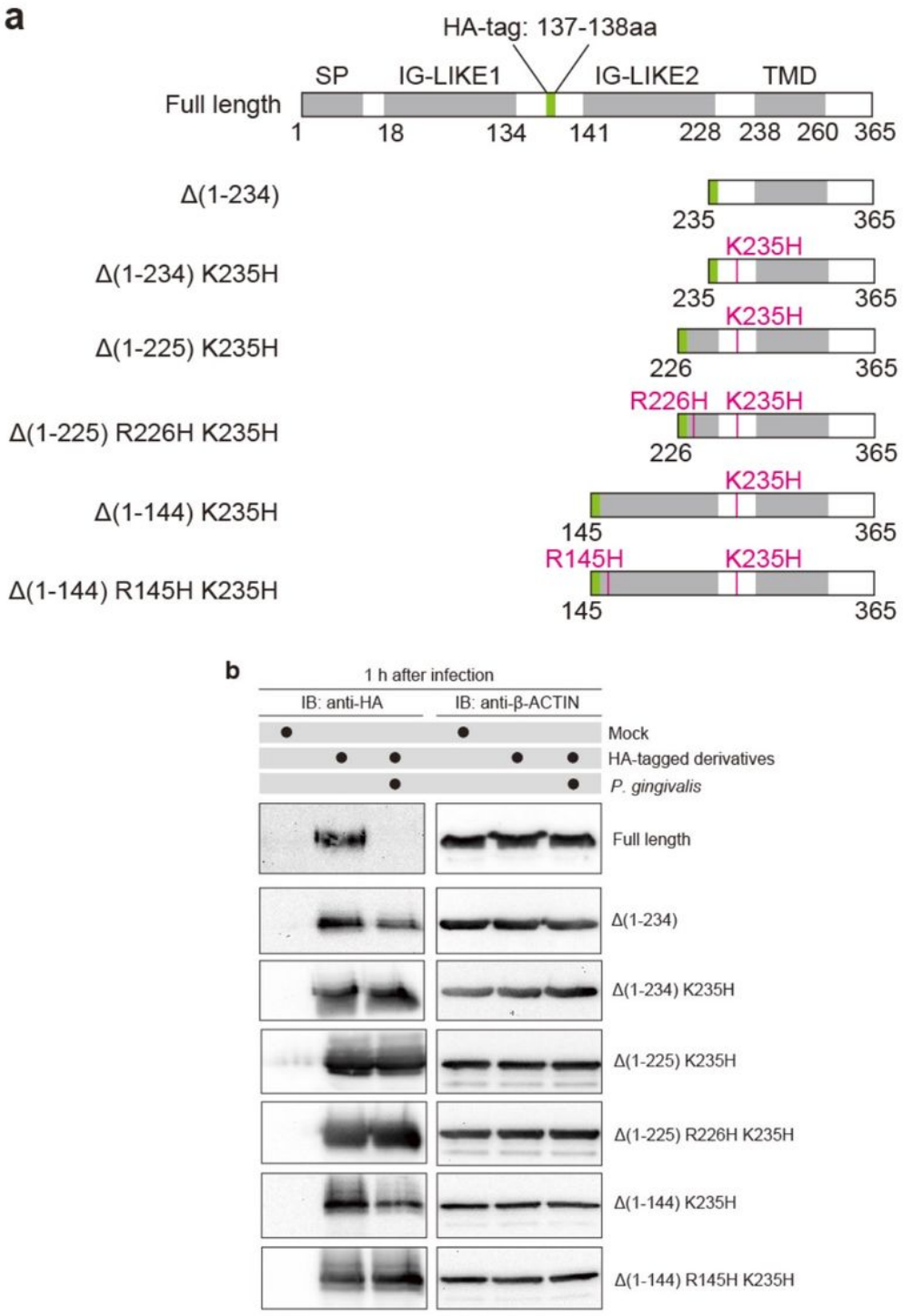

Figure 6

The R145 and K235 residues are targeted for degradation of CXADR by P. gingivalis in IHGE cells (a Schematic view of the CXADR structure and derivatives. SP, IG LIKE, or TMD domains aredomains are indicated byindicated by gray boxes. HAgray boxes. HA–tag tag is is shown in green. The point mutationshown in green. The point mutationss R145HR145H and and K235HK235H are shown in magenta. are shown in magenta. (b(b)) IHGE cells were transiently transfected IHGE cells were transiently

transfected with plasmid with plasmid encoding encoding HAHA––inserted CXADR or the indicated CXADRinserted CXADR or the indicated CXADR mutantmutantss. . Following 48 h of incubation, Following 48 h of incubation, the the cells were infected with cells were infected with P. gingivalisP. gingivalis at an MOI of 100 at an MOI of 100 for 1 hfor 1 h, , andand then analyzed by immunoblotting using the indicated antibodies.then analyzed by immunoblotting using the indicated antibodies.

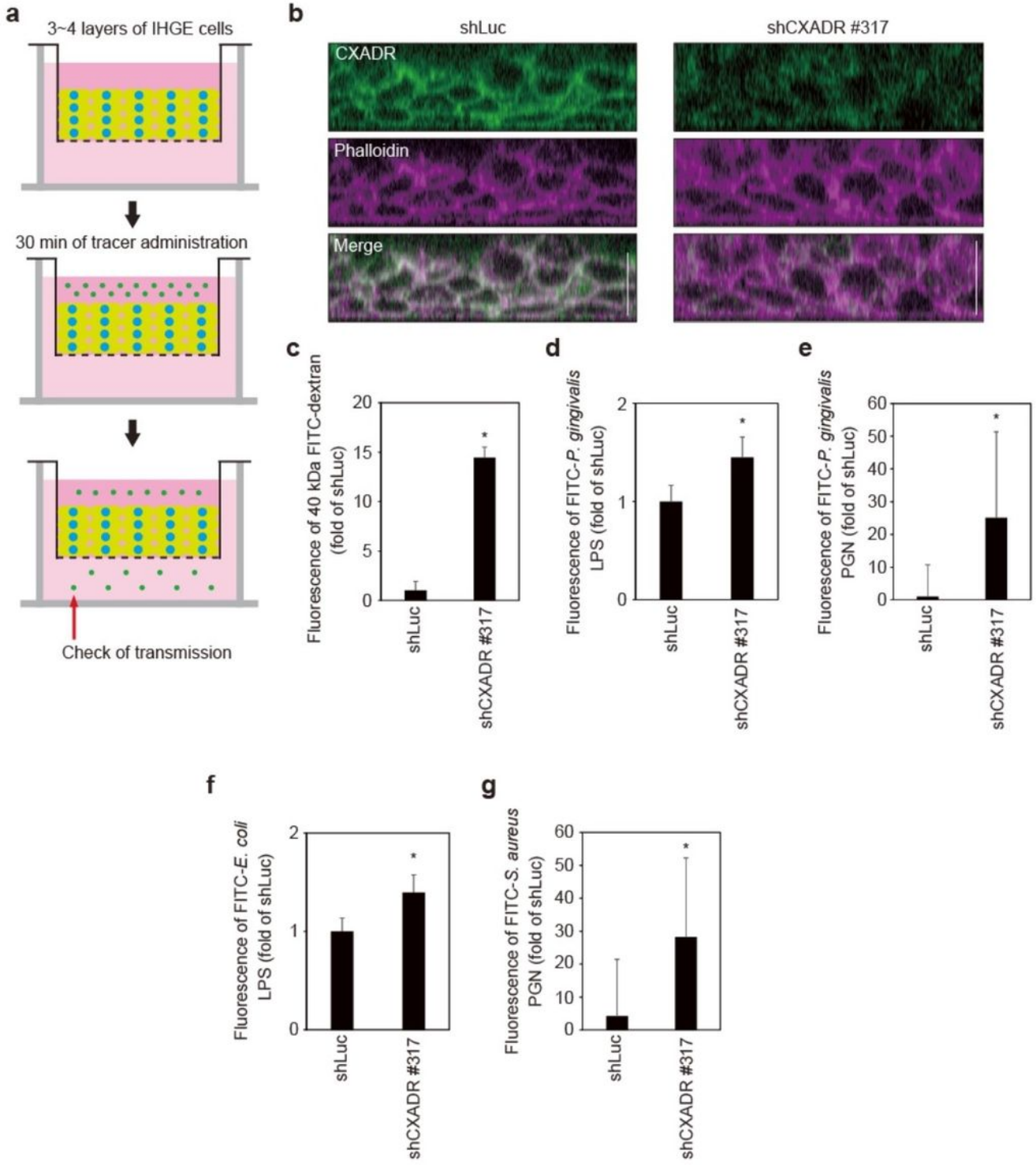

Figure 7

CXADRis required for epithelial barrier function of gingival epithelial tissues. (a,b Schematic illustration (a) and confocal microscopic cross sectional images (b) of 3D tissue model expressing shLuc or shCXADR . Gingival epithelial tissues were fixed, stained with anti stained with anti–CXADRCXADR (green(green) and Alexa Fluor 568) and Alexa Fluor 568––conjugated pconjugated phalloidin (magenta), halloidin (magenta), and analyzed by confocal microscopy. Scale bars, 30 μm.and analyzed by confocal microscopy. Scale bars, 30 μm. (c(c––gg)) Permeability to 40 Permeability to 40 kDa FITCkDa FITC–– dextran (dextran (cc), FITC), FITC––P. gingivalisP. gingivalis LPS (LPS (dd), FITC), FITC––P. gingivalisP. gingivalis PGN (PGN (ee), FITC), FITC––E. coli E. coli LPS (LPS (ff), and FITC), and FITC––S. aureus S. aureus PGN (PGN (gg) in gingival epithelial tis) in gingival epithelial tissues expressing sues expressing shLuc and shCXADRshLuc and shCXADR. Results are expressed as fold . Results are expressed as fold change relative to change relative to epithelium epithelium expressing shLuc and are the meanexpressing shLuc and are the meanss ± SD of ± SD of seven seven technical replicates. *, p<0.05, onetechnical replicates. *, p<0.05, one–– tailed tailed tt test (test (cc––ee).).

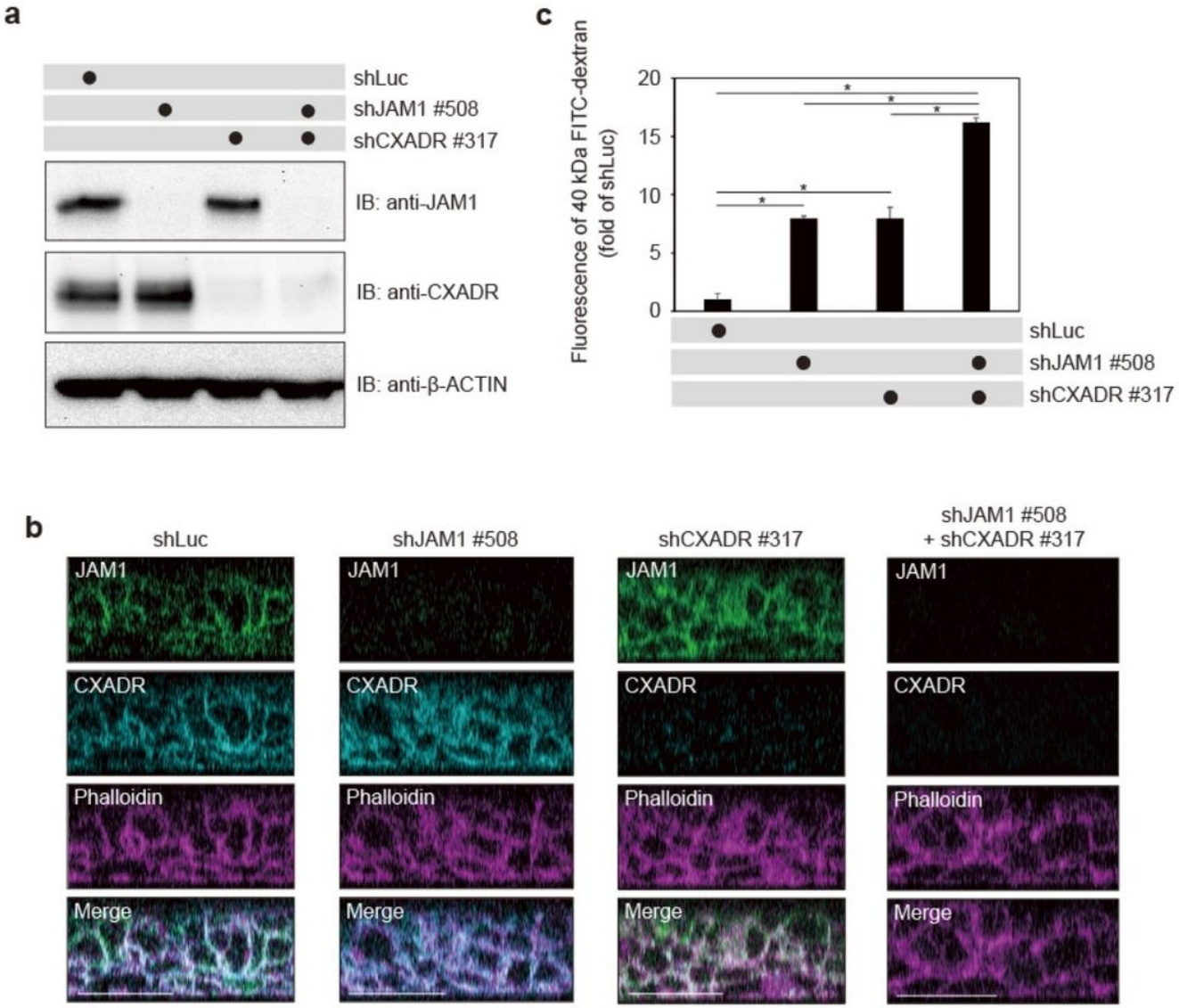

Figure 8

Barrier function in gingival epithelial tissues is regulated by CXADR 705 independently of JAM1. (a IHGE cells stably ex pressing shLuc, shJAM1 #508 , shCXADR #317 , or both shJAM1 707 #508 and shCXADR #317 were analyzed by immunoblotting with the indicated antibodies. (b Gingival epithelial tissues stably expressing shLuc, shJAM1 #508 , shCXADR #317 , or both shJAM1 #508 and shCXADR #317 on coverslips were fixed, stained with anti JAM1 (green), anti CXADR (cy an) and Alexa Fluor 568 conjugated phalloidin (magenta), and analyzed by confocal microscopy. Scale bars, 30 μm. (c Permeability to 40 kDa FITC dextran in gingival epithelial tissues expressing shLuc, shJAM1 shJAM1 #508#508, shCXADR, shCXADR #317#317, or both shJAM1, or both shJAM1 #508#508 and shCXADRand shCXADR #317#317. Results . Results are expressed as fold change relative to epithelium expressing shLuc and are the means ± are expressed as fold change relative to epithelium expressing shLuc and are the means ± SD of eight technical replicatSD of eight technical replicates. *, p<0.05, twoes. *, p<0.05, two–tailed tailed tt test.test.

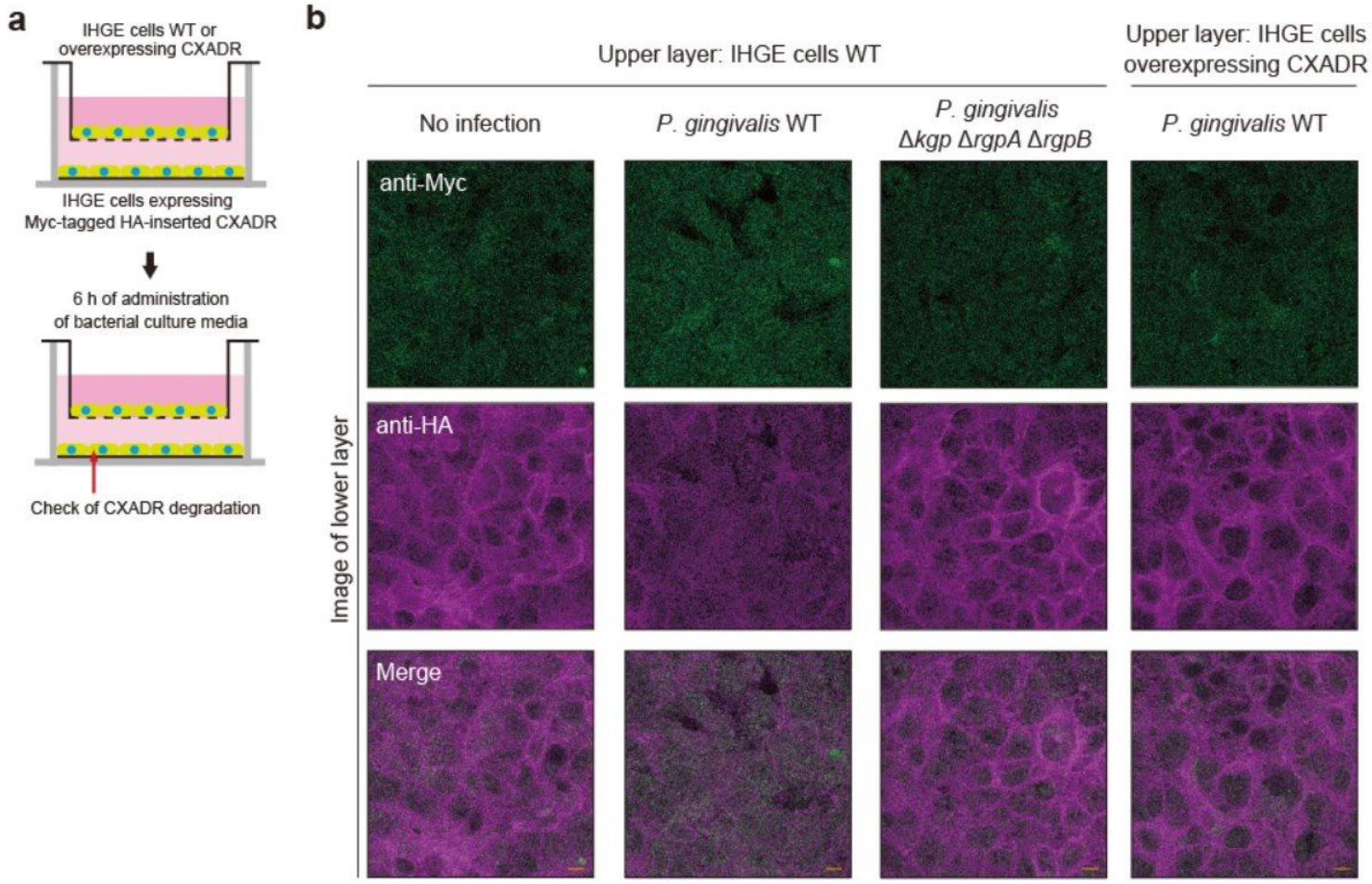

Figure 9

P. gingivalis gingipains penetrate the epithelial barrier of IHGE cells. (a, b Schematic image of the culture insert system (a). Gingival epithelial cell s WT or stably expressing Myc tagged HA inserted CXADR were cultured in the upper compartment and IHGE cells stably expressing Myc tagged HA inserted CXADR on a

coverslip in the lower compartment. The bacterial culture supernatant of P. gingivalis WT or or Δ kgp Δ rgpA Δ rgpB mutan t was administered to cells . Following 6 h of incubation, cells in the lower compartment were fixe d, stained with anti Myc green), and anti HA (magenta), and analyzed by confocal microscopy (b). Scale bars, 10 μm.

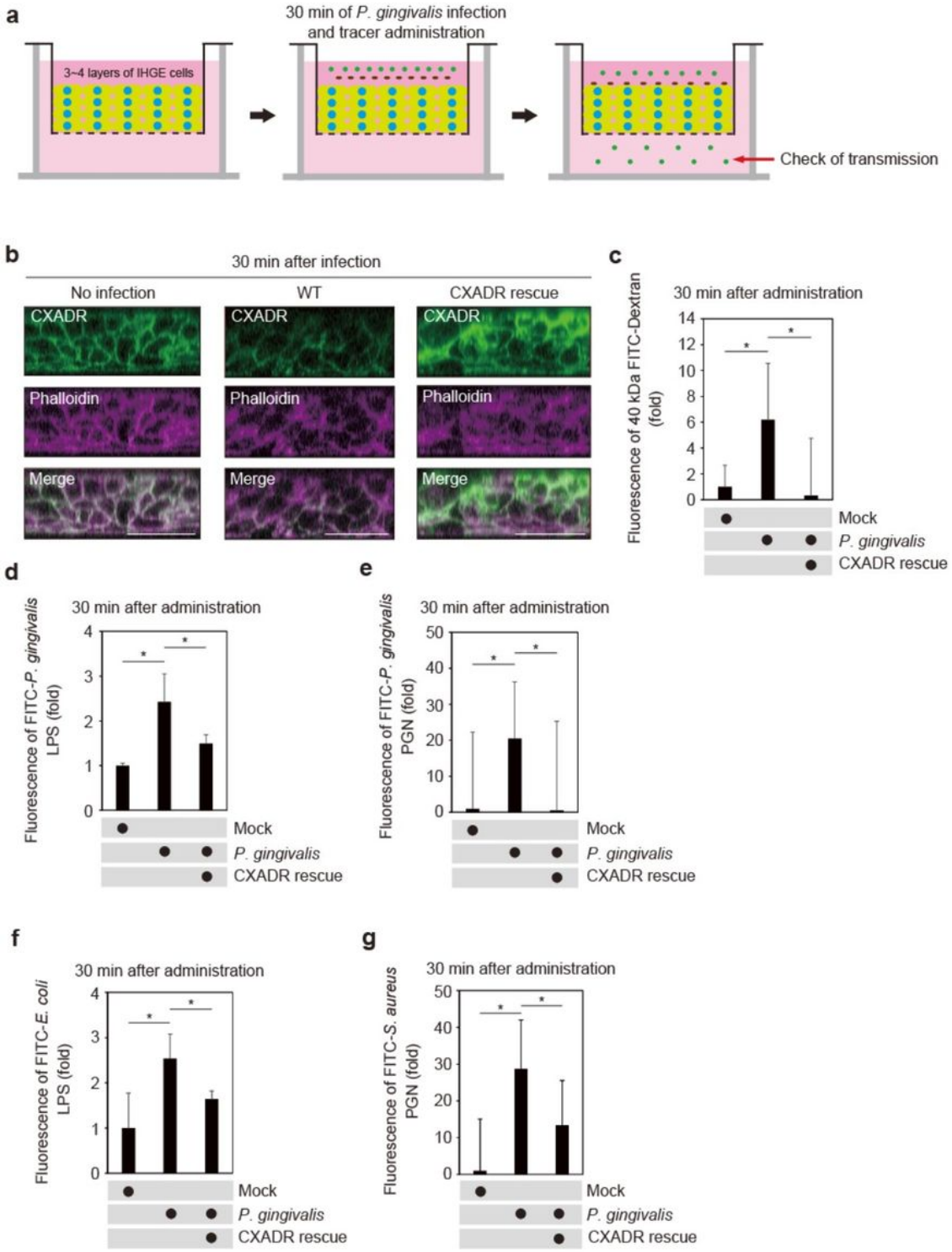

Figure 10

P. gingivalis degrades CXADR of gingival epithelium causing penetration of LPS and PGN. (a,bSchematic illustration of the three dimensional culture (a) and confocal microscopic cross cross–sectional images (sectional images (bb) of the three) of the three–dimensional culture of IHGE cells. Gingival dimensional culture of IHGE cells. Gingival epithelial tissues epithelial tissues ((WT or overexpressing CXADRWT or overexpressing CXADR)) were infected with were infected with P. gingivalisP. gingivalis for 30 for 30 min. Tissuemin. Tissues were ths were then fixed, stained with antien fixed, stained with anti–CXADR (greenCXADR (green) and Alexa Fluor 568) and Alexa Fluor 568––738 conjugatedconjugated pphalloidin (mahalloidin (magenta), and analyzed by confocal microscopy. Scale bars, 30 genta), and analyzed by confocal microscopy. Scale bars, 30 μm.μm. (c(c––gg)) Permeability to 40 kDa FITCPermeability to 40 kDa FITC–dextran (dextran (cc), FITC), FITC––P. gingivalisP. gingivalis LPS (LPS (dd), FITC), FITC–– P. gingivalisP. gingivalis PGN (PGN (ee), FITC), FITC––E. coli E. coli LPS (LPS (ff), and FITC), and FITC––S. aureus S. aureus PGN (PGN (gg)) of of gingival gingival epithelial tissuesepithelial tissues ((WT or WT or overexpressing CXADRoverexpressing CXADR)) infected with infected with P. gingivalisP. gingivalis. . ThreeThree–dimensional dimensional tissues on culture inserttissues on culture insertss were were infected with infected with P. gingivalisP. gingivalis and FITCand FITC–labeled labeled tracer in the upper compartment. Following 30 min of incubation, the tracer in the upper compartment. Following 30 min of incubation, the transmission of transmission of tracer from the upper compartment to the lower compartment was analyzed tracer from the upper compartment to the lower compartment was analyzed by by spectrometryspectrometry. Results are expressed as fold . Results are expressed as fold change relative to uninfectedchange relative to uninfected WT WT cells andcells and are the meanare the meanss ± SD of ± SD of seven seven technical replicates. *technical replicates. *,, $p<0.05$, one$p<0.05$, one–tailedtailed tt test (closed test (closed testing procedure).testing procedure).

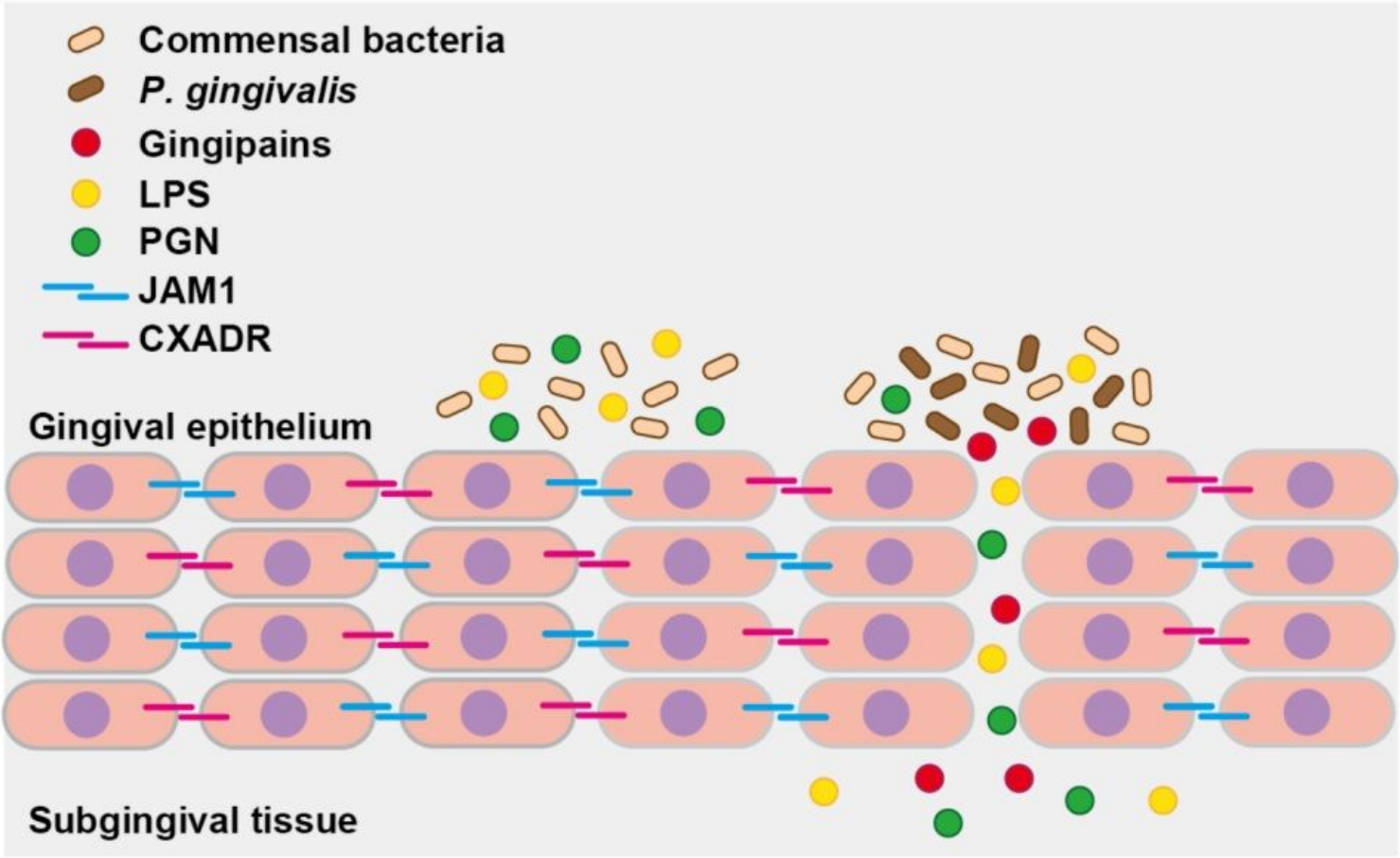

Figure 11

Proposed model of how P. gingivalis gingipains send bacterial virulence factors through the gingival epithelium. In gingival epithelial tissues CXADR (and JAM1 (are not interdependent on the permeability. P. gingivalis gingipains degrade CXADR and JAM1 , which increases the permeability of gingival epithelium to gingipains and other factors .Subsequently, gingipains are transferred to the deeper epithelium to fu rther degrade CXADR and JAM1 , which allows LPS and PGN to penetrate the gingival epithelium and reach subepithelial tissues. Finally, gingipains, LPS, and PGN induce inflammation in gingival tissues.

Supplementary Files

This is a list of supplementary files associated with this preprint. Click to download.

- TakeuchietalSupplementaryInformationver2.pdf